MASTERS OF SCIENCE IN ELECTRICAL AND ELECTRONIC ENGINEERING

Low loss Slotted core photonic crystal fiber for terahertz radiation

Department of Electrical and Electronic Engineering
Islamic University of Technology (IUT)
Board Bazar, Gazipur-1704, Bangladesh
November, 2019

Low loss Slotted core photonic crystal fiber for terahertz radiation

By

Md. Aminul Islam

MASTERS OF SCIENCE

IN

ELECTRICAL AND ELECTRONIC ENGINEERING

Department of Electrical and Electronic Engineering
Islamic University of Technology (IUT)
Board Bazar, Gazipur-1704, Bangladesh
November, 2019

CERTIFICATE OF APPROVAL

The thesis titled "**low loss slotted core photonic crystal fiber for terahertz radiation**" submitted by Md. Aminul Islam, St. No. 152627 of Academic Year 2015-2016 has been found as satisfactory and accepted as partial fulfillment of the requirement for the Degree of **MASTER OF SCIENCE IN ELECTRICAL AND ELECTRONIC ENGINEERING** on 8th November, 2019.

Board of Examiners:

1.

_____

Mohammad Rakibul Islam (Supervisor) — Chairman
Professor,
Electrical and Electronic Engineering Department,
Islamic University of Technology (IUT), Gazipur.

2.

_____

Prof. Dr. Md. Ruhul Amin — Member
Professor and Head,
Electrical and Electronic Engineering Department,
Islamic University of Technology (IUT), Gazipur.

3.

_____

Prof. Dr. Md. Ashraful Hoque — Member
Professor,
Electrical and Electronic Engineering Department,
Islamic University of Technology (IUT), Gazipur.

4.

_____ Member

Dr. Ashik Ahmed
Associate Professor,
Electrical and Electronic Engineering Department,
Islamic University of Technology (IUT), Gazipur.

5.

_____ Member (External)

Dr. Mohammed Imamul Hassan Bhuiyan
Professor,
Electrical and Electronic Engineering Department,
Bangladesh University of Engineering and Technology, (BUET)

DECLARATION OF CANDIDATE

It is hereby declared that this thesis report or any part of it has not been submitted elsewhere for the award of any Degree or Diploma.

_____

Dr. Mohammad Rakibul Islam (Supervisor)
Professor
Electrical and Electronic Engineering Department,
Islamic University of Technology (IUT).
Date:

_____

Md. Aminul Islam
Student No.: 152627
Academic Year: 2015-2016
Date:

ACKNOWLEDGEMENT

First and foremost all the praise is paid to the Almighty, the most kind Allah for keeping me alive and able, giving me the knowledge, ability to think and for helping me to successfully finish my thesis, with His inexhaustible kindness.

The author express his whole hearted deep gratitude, indebtedness appreciation to his honorable teacher, respected supervisor Dr. Mohammad Rakibul Islam, Professor, Department of Electrical and Electronic Engineering, Islamic University of Technology (IUT), Board Bazar, Gazipur, Bangladesh. His continuous assistance, inspiration, guidance and valuable suggestions throughout the period of research work have made this thesis successful. His commitment to excellence has been motivational to me, now and in my future career. I could not have imagined having a better supervisor and mentor for my M.Sc. study.

I am indebted to Dr. Md. Ruhul Amin, Professor and Head, EEE Department, IUT for his valuable support throughout the years of my M.Sc. course.

The author would like to extend his deep sense of gratitude to all of the respective teachers of the Department of Electrical Electronic Engineering, IUT, for their value able suggestions, cooperation and best wishes.

I would like to thank all the students from the papers Zareen Mustafa, Aadreeta Hossain, Tahia Tahsin, Md Moinul Islam Khan, Jubair Alam Chowdhury, Fariha Mehjabin, Mohibul Islam, Zarrin Tasnim, Rakina Islam, Raisa Labiba Khan, Ehtesam Moazzam for their support on my papers. Thanks to my friends and colleagues for their support throughout the research work. Also, I wish to express my sincere gratitude for their suggestions and corrections during thesis writing.

Finally, I acknowledge that this work would be almost impossible to carry out successfully without the inspirations of my parents as they give moral support, optimistic encouragement throughout my research work.

ABSTRACT

Fiber optic systems are important telecommunication infrastructure for world-wide broadband networks. Wide bandwidth signal transmission with low delay is a key requirement in present day applications. Optical fibers provide enormous and unsurpassed transmission bandwidth with negligible latency, and are now the transmission medium of choice for long distance and high data rate transmission in telecommunication networks. Terahertz radiation occupies a middle ground between microwaves and infrared light waves known as the terahertz gap, where technology for its generation and manipulation is in its infancy. The frequency band of 0.1-10 THz, known as THz band has brought potential applications in many important fields. For wave propagation, THz systems use free space as medium. But in free space, waves face many difficulties which is very big issue for wave propagation. So we have to use guided transmission instead of unguided transmission. Our main objective is to design an optical waveguide which will be able to transmit terahertz signal into longer distances. Low material loss and high core power fraction is major concern for designing a Terahertz photonic crystal fiber. Material loss occurs due to the use of bulk material in the background of photonic crystal fiber. Several ultra-low loss terahertz (THz) photonic crystal fibers (PCF) design have been proposed and inquired precisely. We proposed four photonic crystal fiber designs where two is slotted air hole inside the octagonal core, another one is slotted air hole inside the hexagonal core and finally last one is a circular air hole inside hexagonal core. All the simulations are performed with Finite Element Modeling (FEM) package, COMSOL 5.3b. The design can be fabricated using stack and drilling method. The investigation results have proved that the designed PCFs shows very low effective material loss (EML) such as 0.010 cm^{-1}, 0.012 cm^{-1}, 0.025 cm^{-1} and 0.029 cm^{-1}, at 2.1THz, 1.6 THz, 1.6 THz and 1.7 THz respectively. The core power fractions of those proposed design are 70%, 60%, 50% and 49% respectively. Moreover, other optical parameter of those PCF such as effective mode area (EMA), confinement loss (CL), and dispersion have been investigated also. The proposed PCFs suggested flatted dispersion from 0.70 THz to 2.10 THz, 0.60 THz to 1.60 THz, 0.60 THz to 1.60 THz and 0.50 THz to 1.70 THz. The outcomes indicate that the proposed PCFs will be good candidates for THz or T-ray transmission as well as in the area of photonic devices also.

Dedication

My respected Parents and adorable Wife

“Without whom none of my success would be possible”

Table of contents

List of Figures

List of Abbreviations

EML: Effective Metarial Loss

FEM: Finite Element Method

GVD: Group Velocity Dispersion

ITU: International Telecomunication Union

LED: Light Emmiting Diode

MPOF: Microstructure polymer optical fiber

MTIR: Modified Total Internal Reflaction

PBG: Photonic Band Gap

PCF: Photonic Crystal Fiber

PC-PCF: Poras Core Photonic Crystal Fiber

PML: Perfactly Matched Layer

PMMA: Polymethyl Methacrylate

SMF: Single Mode Fiber

THF: Tremendously high frequency

THz: Terahertz

TIR: Total Internal Reflection

VCSEL: Vertical Cavity Surface Emitting Laser

PMC: Perfact magnetic conductor

PEC: Perfact electyric conductor

FDM: Finite difference method

MOF: Microstructure optical fiber

FDTD: Finite difference time domain

Nomenclature

v	Normalized frequency
η_{co}	Refractive index of core
η_{cl}	Refractive index of cladding
n_{mat}	Refractive index of Topas,α_{mat}
α_{mat}	Bulk material absorption loss
ε_0, μ_0	Permittivity, permeability
η	Mode power fraction
α_{eff}	Effective material loss
f	Frequency of the guiding light, c is and symbolizes the
c	Speed of light in vacuum
I_m(neff)	Imaginary part of the refractive index
α_{cl}	Confinement loss
χ_e	Electric susceptibility
ω(β	Angular frequency)
β	Propagation constant
$I(r)$	Transverse electric intensity distribution
A_{eff}	Effective area
B	Birefringence
n_x	Refractive index of x pol
n_y	Refractive index of y pol

Chapter 1

Introduction

In this Chapter, we present an overview of our thesis that demonstrates the motivation behind this work. To the concurrent and earlier technology adopted to mitigate the effective material loss, which is the central part of this research work, has been noticeably focused in this chapter. In section 1.1 we illustrate the background of our research works. Then in section 1.2, 1.3, 1.4 and 1.5 discuss about the literature review, the summery of limitations, Thesis objective and possible outcomes respectively. Finally we end the chapter with the description of thesis overview in section 1.6.

1.1 Background

In recent years, enormous efforts have been paid to THz PCFs due to lots of applications in different fields including remote sensing, imaging, security screening and THz time domain spectroscopy. Development of low-loss and low dispersion THz PCFs enable variety of promising applications in Biomedical technology such as non-invasive early diagnosis of skin cancer including the basal cell carcinoma, dysplastic skin nevi and melanomas of hardly-accessible skin areas [5]. For propagate the THz waves free space medium are used in the communication system, this is for creates various types of problems. Lots of barrier displayed for efficient transmission of THz wave, such as strong water vapor absorption, misalignment issues and complex integration with other components etc. now a days researchers doing hard work to develop various forms of waveguide structures to overcome these problems. However, due to the challenge of dealing with excessive absorption loss, the commercial production of efficient THz waveguide is lagging behind. A great deal of numerical and experimental researches has been performed in order to increase the reliability during the transmission of broadband THz waves through a guiding structure. Now a day's remarkable success has been achieved in optics sector of the guiding properties of THz fibers by using comparatively smaller air holes (smaller than operating wavelength) in the core of the PCF. This type of structure are porous-core PCFs. Porous-core PCFs have gained increased attention due to freedoms for tuning EML, dispersion and confinement loss in a smart way [8]. The wave propagation through porous-core PCF is based on the non-absorbing nature of dry air [9]. Using this formulation, making a tight light

confinement in the core and sending most of the mode power into the porous-air holes can greatly reduce the absorption and confinement loss. For example, the theoretical characteristics and experimental measurements of groove guide structure have been demonstrated for low-loss THz signal transmission [10]. A porous-core honeycomb THz fiber has been proposed by [19] that exhibited low material absorption loss of 1.5 dB/cm at 1.0 THz. However, maintaining of periodicity during the fabrication of honeycomb structure is too difficult. Porous-core octagonal PCF has been reported [20] that showed low EML of 0.07 cm-1 at 1.0 THz. In this work, the authors have not considered few crucial guiding characteristics such as dispersion and power fraction. A hexagonal PCF with hexagonal porous-air holes has been proposed in [21], where the reported EML was comparatively higher about 0.12 cm^{-1}. Very recently, a porous-core kagome lattice PCF has been reported in [22] using hexagonal lattice air-holes in the core. This PCF showed very low EML of 0.035 cm-1 at 1.0 THz. However, owing to complex structure fabrication of kagome lattice PCF is limited. The structures proposed in Refs. [23–25] also represent noticeable improvement in terms of EML, confinement loss and power fraction. Although promising porous core PCFs have been proposed based on the triangular lattice, a square lattice PCF has never been reported in the literature. Therefore, it is quite interesting to observe how the guiding properties of square lattice differ from a regular triangular lattice. The square lattice PCF permits easy fabrication process since it can be realized with standard stack and draw technique [26, 27]. Moreover, technological feasibility of the square lattice PCF has already been demonstrated in [28].

1.2 Literature Review

This chapter focused on lots of terahertz photonic crystal fiber design and their results from the previous and recent research works. Many researches have been made on Photonic Crystal Fiber and those researches modified the PCF technology. In 1978, the Idea of Bragg fibers that revolutionized the telecom with components sensors and filters but the major drawbacks encountered were large no modes travelling in it, their huge size and greater loss [1]. Later in 1992 the fiber design include the mechanism of Total Internal Reflection with a good perforation in telecommunication except with few problems like limited material choice, limited core diameter for Single Mode Operation [2]. The photonic coated fiber were fabricated in 1996 with additional feature of increased durability, high strength designed, high

temperature resistance accordingly use in nuclear radiations, harsh chemical environments, Medical applications etc.

1.2.1 Zeonex based research works of elliptical core hexagonal photonic crystal fiber.

Since the terahertz region is situated between the technologically well-developed microwave and infrared regions, it is amenable to generation and detection techniques from both fields. The interest in terahertz technology is also growing because of its numerous potential applications. However, the practical implementation of terahertz is limited because most of terahertz transmission systems are bulky and mostly dependent on free space for wave propagation. In the case of free space propagation, a number of undesirable losses can be introduced due to coupling with other components, transporting and managing of terahertz beams etc. As a primary solution, prior studies have proposed several waveguides including parallel plates, metallic wires, metal coated dielectric tubes, polystyrene foams, sub-wavelength polymer fibers, Bragg fibers, and hollow core fibers [4, 5, 6]. These all possess shortcomings due to higher absorption loss, higher coupling loss, lower power fraction, and higher bending loss. As an improvement, porous core PCF [7, 8, 9, 10, 11] has gained considerable attention because of its versatility in enabling desired wave guide properties. Note that a PCF's geometrical parameters such as core diameter, core air hole size and shape, distance between air holes, frequency can be tuned and optimized to obtain desired properties that enables low loss, controllable chromatic dispersion, high birefringence, and large modal effective area. There are several studies that considered micro-structured porous core fibers for operation in terahertz band. In 2008 and 2009, Atakaramians et al. experimentally characterized porous core PCFs of different geometries [12.13]. Using zeonex as the background material, they obtained a low birefringence with high dispersion variation in terahertz frequency band. Later studies examined a dual air hole unit based PCF and showed a moderate birefringence of 0.033 [14]. Next, without significant improvement in birefringence, dual asymmetrical based PCF's were also proposed [15, 16]. Furthermore, Wu et al. proposed a PCF and obtained a low birefringence with high dispersion variation [17]. But they do not consider the effective material loss and also the confinement loss.

1.2.2 Topas based research works of slotted core hexagonal photonic crystal fiber.

Recent years many researchers proposed slotted-core PCF incorporating a hexagonal cladding. They proposed fiber exhibits simultaneously low birefringence and high effective absorption

loss. Also Slotted fibers with air-cladding, [18] and circular lattice cladding were reported earlier [21]. But they do not consider the dispersion and effective area. Atakaramians et al. designed and fabricated a porous fiber [17], [18] with rectangular air-holes that showed a high birefringence of-O.012 at 0.65 1Hz. Chen et al. proposed a squeezed lattice elliptical-hole 1Hz fiber [19] with a birefringence of the order 10^{-2}. A plastic based PCF [20] showed high birefringence of -0.021, but the reported propagation loss was very high. In 2013, Chen et at. offered a porous fiber with rotated elliptical air-holes [6]. It showed a high birefringence of -0.045 and a very high effective absorption loss. Most recently, Islam et al. proposed a slotted core PCF [21] with circular lattice cladding that exhibited a high birefringence of -0.075 with a low transmission loss. Nevertheless, all these works mentioned in the literature used either solid air-cladding [10, 17-19] or complex lattice holey cladding [21]. These factors cause high absorption loss, coupling with external environment and fabrication difficulties resulting in an overall degradation of the performance of the fiber. A large number of papers have been published. In 2009, Chen et al. [12] proposed a diamond shaped PCFs that exhibit a birefringence of 1.0×10^{-2}which is comparatively low. Islam et al.13showed a slotted core PCF that demonstrates a birefringence order of 7.5×10^{-2}. But, the effective material loss (EML) is 0.07 cm^{-1} which is comparably higher. Using slotted core kagome THz fiber, a research showed a birefringence order of 8.22×10^{-2} and EML of 0.05 cm^{-1}. However, Cho et al. established a plastic-based fiber [15] that showed a birefringence of 2.1×10^{-2} with a propagation loss 400 dB/m which is very high. Elliptical [16, 17] and rectangular air holes [18, 19] were used to achieve a birefringence in the order of 10^{-2} but it can lead to a loss about the order of 400 dB/m. but in 2015, Islam et al. proposed a solid cladding structure that interacts directly with the environment which may lead to a high loss medium. However, metallic [20] and polymer [16, 18, 21, 22] waveguides were introduced earlier. Chen et al. proposed a rotational core with solid air cladding that depicts a birefringence order of 0.045. Squeezed lattice, [22] rectangular slotted core [16–18] based PCF were reported with birefringence of 0.026. Polymer tubes [23, 24] showed a high birefringence with high loss structure. The former depicted that slotted core waveguides [16,18] showed a birefringence of 0.026 with a high loss of 0.07 cm^{-1}. Islam et al. [25] proposed a diamond-core porous fiber which exhibits a birefringence of 10^{-2} and EML of 0.07 cm^{-1}. [26] Demonstrated a polarization maintaining slotted core kagome structure which depicts a birefringence of 8.22×10^{-2} and EML of 0.05 cm^{-1}. Later, Islam et al. [29] demonstrated

an asymmetric slotted core crystal fiber which reports the birefringence of 7.5×10^{-2} and EML of 0.07 cm^{-1}. Later [27] demonstrated a porous-core THz PCF which represents a birefringence of 1.32×10^{-2}. In 2016,Wuet al. represented an oligoporous-core [28] THz PCF which exhibits a birefringence of 3×10^{-2}. But the confinement loss (CL) increases when core porosity increases. This is a negative outcome of this experiment. In 2018, Foisal et al. experimented with elliptical core with slotted air holes [29] and obtained a birefringence of 1.057×10^{-1}, EML of 0.047 and CL of $9.4\times10{-}3cm^{-1}$. Later in 2018, Sultana et al. [30] showed an elliptical core PCF with a birefringence of only 0.086. Also in 2018, Habib et al. [31] proposed a structure with a birefringence in the order of 10^{-2} and EML is of 0.07 cm^{-1}.

1.3 Summary of limitations of the existing models of terahertz photonic crystal fiber.

From the literature review of the existing design of Zeonex and Topas based terahertz photonic crystal fiber, it can be inferred that there are some limitations.

- There are some papers which they founding only on the birefringence of photonic crystal fiber but confinement loss issue is ignored in that work.
- On the other hand, in some designs, even though a good result is obtained for very small frequency range.
- Most of the paper proposed Topas based photonic crystal fiber and they exhibits outstanding results but the common limitation is that the effective material loss optimization is not up to quantity.
- Research work in being carried out for new design of the terahertz photonic crystal fiber for reduce the effective material loss and get it more flatten dispersion properties.

1.4 Thesis Objectives

The past few years researchers concentrate their focus on terahertz spectral range (1011 to 1013 Hz) lying between microwaves and infrared bands. THz range has lots of applications. Hence, present terahertz developments are limited to free-space applications, to designing a THz photonic crystal fiber which have lots of challenges such as alignment difficulties, path loss, and uncertain absorption loss. The main obstacle for designing a terahertz waveguide is the high material absorption loss of the background material. It is possible to reduce the loss by increasing

the core power fraction and maintaining tight confinement between the air holes of the core. The main objective of my research work is to design a porous based slotted core photonic crystal fiber to transmit high frequency THz signal efficiently into longer distances with high core power and low material absorption loss. The overview of this research work is given as follows:

- To reduce the material absorption loss
- To get the maximum confinement.
- To get maximum core power fraction.
- To develop a flatten dispersion photonic crystal fiber.
- To design a single mode fiber.

1.5 Possible outcomes

Outcome of this research will be as follow.

- Effective material absorption loss will be less than 0.030 cm^{-1}.
- Confinement loss will be almost 10^{-16} cm^{-1}.
- Core power fraction will be more than 50%.
- Normalized frequency (V-parameter) will be less than 2.40.

1.6 Thesis Organization

Our paper is organized as follows.

- Chapter 1 signifies the background, literature review and objectives with specific aims.
- Chapter 2 illustrates the basic theory of PCF
- Chapter 3 Physical construction of PCF and THz Band
- Chapter 4 Design methodology and simulations of proposed PCFs.
- Chapter 5 Illustrate details about different factors and results of proposed PCFs
- Chapter 6 represents the conclusion.

Chapter 2

Basic theory of PCF

This chapter provides the background information necessary to understand the modeling work done in this thesis. Commonly used methods for modeling of optical fibers cannot be applied successfully in photonic crystal fiber (PCF) modeling. These fibers have a high refractive index contrast and a sub-wavelength periodical structure. Therefore, the methods used in modeling photonic crystals and electromagnetic fields are adopted for this purpose. The chapter starts with an overview of the differential mathematical problem that needs to be solved in order to study light propagation in a microstructure optical fibers (MOFs) then the principal simulation methods so for developed for the study of MOFs. The choice of the finite element method (FEM) as the preferred method for the transmission studies in PCF.

2.1 Numerical Techniques

There are various numerical methods to find the solutions of Maxwell's equations derived for the MOF. Since MOF exhibits higher index difference between core and cladding, the electromagnetic analysis eventually turns complex. The methods normally used for conventional fibers are less likely used in MOF as they provide only the approximate solutions. Maxwell's vector equation which is used in the analysis of MOFs is written as,

$$(\nabla^2 + k^2\varepsilon(rT) + [\nabla \ln\varepsilon(rT)] \wedge \nabla \wedge)HT = \beta^2 HT \qquad 2.1$$

Where $\varepsilon(rT)$ is the dielectric constant rT is position in the transverse plane, $k = \omega/c$ is the wave vector. The scalar approximate of Eq. (2.1) is given as

$$\nabla^2 HT + [k^2\varepsilon(rT) - \beta^2]HT = 0 \qquad 2.2$$

For solving the Eigen value Eq. (2.1) or (2.2), various methods have been reported. The choice of the numerical techniques would depend on the fiber geometry. Some techniques rely on their symmetry to increase the accuracy of the solution and a few other methods provide better solution for highly periodic structure but with less complexity. If the MOF has perfect circular holes, multiple methods is the best and fastest method, White Gaussian functions are used in

the expanding fields that result in solution for Eq. (2.1). The next accurate method is the finite difference time domain (FDTD) technique. But, it requires a large memory space for solving higher dimension fiber structure. A relatively less frequently used approach is the source-model technique which uses two sets of elementary sources to determine the field both inside and outside the silica regions. Finally, the fastest and versatile method for complex structure is the finite element method (FEM) which is discussed in detail in the next section. The above discussed methods are used to analyze the field distributions in the PCF.

2.2 Method of mode analysis

In mode-solving analysis, the values of β or n_{eff} and the corresponding electric or magnetic fields are to be determined by solving the governing wave equation, which is practically an eigenvalue problem. One way to solve it numerically is by translating the partial difference equation or ordinary differential equation into a system of algebraic equations through discretization. Hence the problem becomes a matrix eigenvalue problem with β_2 or n^2_{eff} as the eigenvalue and the corresponding modal field as the eigenvector. The numerical methods developed within this work are based on this approach. In this sub- section, we will briefly introduce these numerical methods, i.e. finite difference method (FDM) and FEM, which will be used in other chapters of this thesis. For simplicity, we will initially consider structures with 1-D cross-section to illustrate the methods. Later on, we will also briefly show the extension into 2-D cross sectional problem by using the FEM and the effective index method.

2.2.1 Finite element method

Finite element method is a general and proven technique for the engineering applications like structural analysis. It is an appropriate tool for solving the partial differential equations. When compared to other numerical methods, FEM provides relatively more accurate solutions for complex shapes and structures. Basically it involves the following four steps

- Discretizing the solution region into finite number of sub-regions
- Deriving the governing equations for a typical equation
- Assembling all the elements in the solution region
- Solving the system of equations

2.2.2 Finite element formulation for MOFs

The FEM is a full-vector analysis suitable for modeling MOFs with large air-holes and high-index variations, and also for accurately predicting their properties [12]. Perfectly matched layer (PML) is the boundary condition that is used for the analysis of MOFs. As a first step in FEM, the fiber cross-section is divided into small segments using any one of the FEM meshing elements. Fig. 2.1 shows the subdivided cross section of PCF using triangular elements. In FEM, there are different types of meshing elements such as linear, quadratic and cubic ones. The elements can be chosen according to the shape of the structure and the required accuracy of the solution. The Eq.2.2 can also be written as [13].

$$\Delta \times (n^2 \Delta \times H) - K_0^2 = 0 \qquad 2.3$$

Where n is the refractive index and k0 is the free space wave number. By applying the Garlerkin's or FEM procedure the Eq. 2.3 becomes,

$$[M]\frac{d^2ht}{dz^2} - 2jn_0k_0[M]\frac{dh_t}{dz} + ([K] - n_0^2k_0^2[M])h_t = 0 \qquad 2.4$$

By assuming the z directive terms in Eq. (2.4) to zero, we obtain the following eigenvalue equation

$$[K]h_t = n_0^2k_0^2[M]h_t \qquad 2.5$$

where [K] and [M] are the finite element matrices, h is the discretized magnetic field vector consisting of the edge and nodal variables. The matrices [K] and [M] are sparse allowing an efficient resolution of the equation by means of high performance algebraic solvers for both real and complex problems. To save computational efforts, structural symmetries can be exploited in the numerical simulations. Also to increase the speed of simulation and to improve the accuracy of the field values, one-quarter of the fiber cross section can be used for the meshing, which is shown in Fig. 2.1. The next important step is to choose the solver which can solve the set of linear equations. There are variety of solvers used in FEM, the choice of which would depend on the required accuracy and the available memory space. Recently a number of commercial packages have appeared that could solve Maxwell's equations using a finite element combined with fast matrix eigenvalue solvers. For e.g. COMSOL.

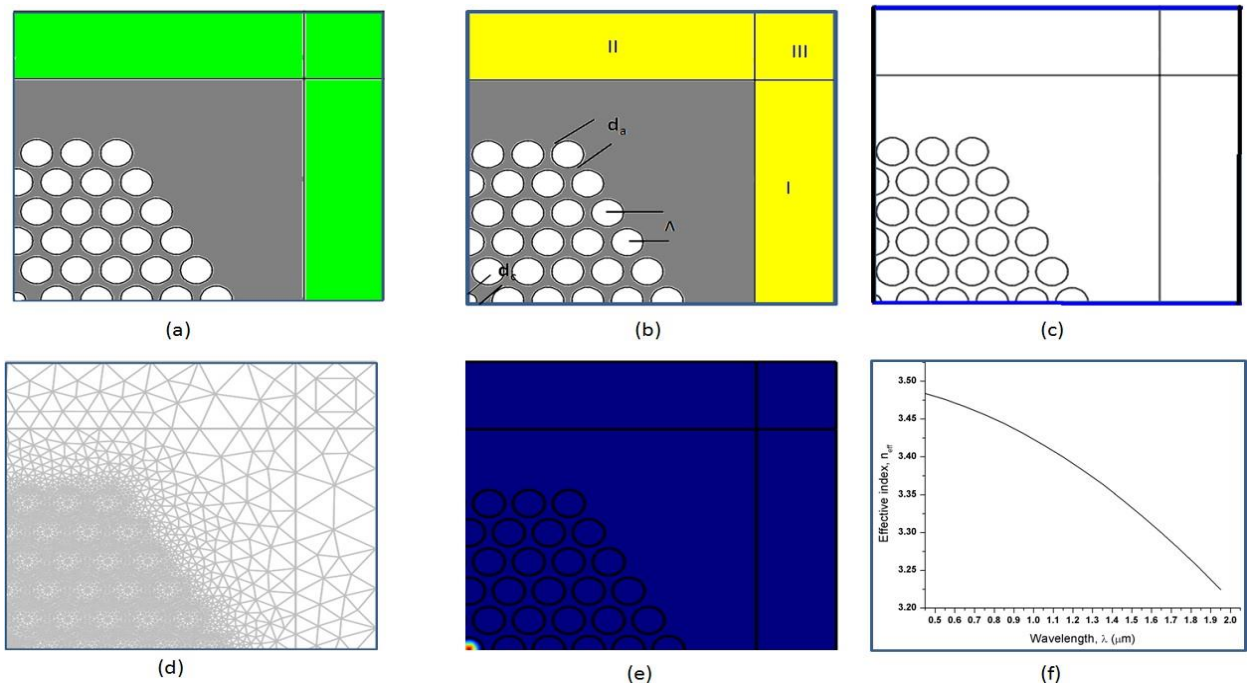

Figure 2.1: Example of FEM simulation: (a) Structural design; (b) Subdomain definition; (c) Setting of the boundary condition; (d) Mesh generation; (e) Post plotting; (f) Computed effective index curve

Multiphysics is a powerful FEM package which combines different domains in the simulation. In order to enclose the computational domain without affecting the numerical solution, anisotropic PMLs are placed before the outer boundary. This is discussed in detail in the next subsection.

2.3 Perfectly matched layer

From the implementation point of view, it is more practical to describe the PML as an anisotropic material with losses. The PML can have arbitrary thickness and it is assumed to be made of an artificial absorbing material. The material has anisotropic permittivity and permeability that match the permittivity and permeability of the physical medium outside the PML in such a way that there are no reflections [15]. The Fig. 2.1 represents schematic diagram of transverse cross section of a PCF surrounded by PML regions at the edges of the computational window, where x and y are the transverse directions and z is the propagation After all, research work in being carried out for new design of the terahertz photonic crystal fiber for reduce the effective material loss and get it more flatten dispersion properties.

PML parameter	Region I	Region II	Region III
α_x	α	1	α
α_y	1	α	α

Table 2.1: Parameters α_x and α_y

Direction. PML regions I and II are defined by the x and y directions, respectively. Re- gions III correspond to the four corners and 'W' is width of the PML. The del operator ∇ in Eq.(2.6) is defined as

$$\nabla = \hat{x}\, a_x \frac{\partial y}{\partial x} + \hat{y}\, a_y \frac{\partial y}{\partial x} + \hat{z}\, a_z \frac{\partial y}{\partial z} \qquad 2.6$$

Here, the α_x, α_y and α_z are related to the PML boundary conditions applied at the edge of the computational window. The αs are determined using the by equation 2.7 [16].

$$\alpha = 1 - j\, \frac{3\lambda\tau\rho_d^2}{4\pi n W^3} \ln\left(\frac{1}{R_T}\right) \qquad 2.7$$

Where ρ_d is the distance inside the PML measured from the interface between the PML and the edge of the computational window and R_t is a theoretical reflection coefficient at the interface between the PML and the edge of the computational window. The permittivity and permeability tensors in the PML region are expressed by equation 2.8

$$[\varepsilon]PML = \varepsilon_0 n^2\,[L],\ \ [\mu]PML = \mu_0\,[L] \qquad 2.8$$

Where ε_0 and μ_0 are permittivity and permeability of free space and n is the refractive index with

$$\begin{bmatrix} \frac{\alpha_y \alpha_z}{\alpha_x} & 0 & 0 \\ 0 & \frac{\alpha_z \alpha_x}{\alpha_y} & 0 \\ 0 & 0 & \frac{\alpha_x \alpha_y}{\alpha_z} \end{bmatrix}$$

The PML parameters αx and αy are given in Table 2.1, and α_z will be unity where the wave propagation is assumed to be along the z direction.

Chapter 3

Physical construction of PCF and THz Band

Photonic crystal fiber (PCF) is a kind of optical fiber that uses photonic crystals to form the cladding around the core of the cable. Photonic crystal is a low-loss periodic dielectric medium constructed using a periodic array of microscopic air holes that run along the entire fiber length. In PCFs, photonic crystals with photonic band gaps are constructed to prevent light propagation in certain directions with a certain range of wavelengths. Contrary to normal fiber optics, PCFs use total internal reflection or light confinement in hollow core methods to propagate light. Light propagation in PCFs is far superior to standard fiber, which uses constant lower refractive index cladding. Applications for photonic crystal fibers include spectroscopy, metrology, biomedicine, imaging, telecommunication, industrial machining and military technology. Photonic crystal fiber is also known as microstructure fiber.

3.1 Background

The term photonic crystal fiber was first coined by Phillips St. J. Russel in the early 1990s [4]. These are the kind of fibers that offer new and improved features and overcome the limitations of the conventional optical fibers. Its geometry is such that there is a periodic arrangement of air holes that run throughout the fiber length. In the beginning hexagonal photonic crystal fiber structure was designed. With the passage of time, due to advancement in the fabrication technology many new structures such as triangular, circular, square, octagonal, hybrid, decagonal and honeycomb PCF is designed to obtain decent guided properties. To improve the performance of the photonic crystal fiber structures different materials such as silica, tellurite, Teflon, PMMA and Topas are used. As a result, due to advancement in the fabrication technology PCF results in low confinement loss, high sensitivity, high numerical aperture, high nonlinearity, large mode area, highly birefringence, ultra-flattened dispersion, zero flat dispersion and low bending loss [5]. This can be achieved by changing PCF parameters namely lattice pitch and hole diameter. Thus these fibers combine the properties of conventional fibers and photonic crystals and thus possess unique properties which make them superior to the conventional optical fibers. In comparison to optical fibers, photonic crystal fiber offer design flexibility. Generally, for

simplicity, most of the photonic crystal fiber are fabricated using silica glass with n = 1.45. There are two guidance mechanisms depending on the PCF geometry. It includes (1) Index guided fiber or holey fiber, (2) Photonic band gap fiber. Index-guided fiber consists of the solid core where light is guided by the modified total internal reflection whereas photonic band gap fiber has a hollow core and follows photonic band gap mechanism. PCF are widely used in Spectroscopy, Metrology, Ophthalmology and imaging and in many other applications.

3.1.1 Construction

Generally, such fibers are constructed by the same methods as other optical fibers: first, one constructs a "preform" on the scale of centimeters in size, and then heats the preform and draws it down to a much smaller diameter (often nearly as small as a human hair), shrinking the preform cross section but (usually) maintaining the same features. In this way, kilometers of fiber can be produced from a single preform. The most common method involves stacking, although drilling/milling was used to produce the first

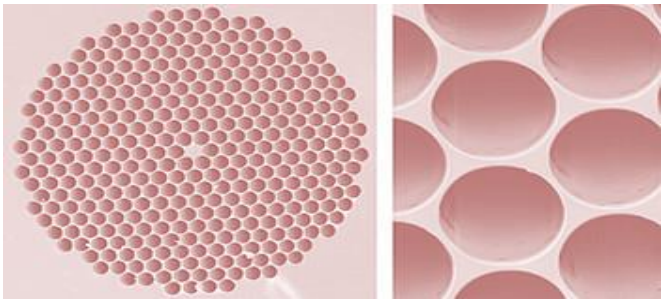

Figure 3.1 Photonic crystal fibers

Aperiodic designs. [7] This formed the subsequent basis for producing the first soft glass and polymer structured fibers. Most photonic crystal fibers have been fabricated in silica glass, but other glasses have also been used to obtain particular optical properties (such as high optical non-linearity). There is also a growing interest in making them from polymer, where a wide variety of structures have been explored, including graded index structures, ring structured fibers and hollow core fibers. These polymer fibers have been termed "MPOF", short for microstructure polymer optical fibers (van Eijkelenborg, 2001). A combination of a polymer and a chalcogenide glass was used by Temelkuran et al. (2002) for 10.6 μm wavelengths (where silica is not transparent).

3.1.2 Guiding Mechanism

In standard optical fiber total internal reflection is the method of guiding light since core refractive fiber the two light-guiding mechanisms is used. In solid-core photonic crystal fibers, where light is confined in a higher refractive index region, modified total internal reflection is exploited, which is quite similar to the guiding mechanism of standard optical fibers. Instead, when the light is confined in a region with a refractive index lower than that of the surrounding area, as in hollow-core fibers, it is due to the presence of the photonic band gap.

A. Modified Total Internal Reflection It is possible to use a two-dimensional photonic crystal as a fiber, by choosing a core material with a higher refractive index than the cladding effective refractive index. An example of this kind of structures is the PCF with a silica solid core surrounded by a photonic crystal cladding with a triangular lattice of air-holes. These fibers, also known as index-guiding PCFs, guide light through a form of total internal reflection (TIR), called modified TIR. Basically in solid core PCF, core consists of pure silica whereas cladding contains photonic crystal which has number of air holes that decreases the refractive index of core. This modified refractive index of cladding which is less than that of core enable light to travel using phenomenon of modified total internal reflection. We can better understand the guiding mechanism by comparing it to model filter or sieve. The cladding of PCF consists of air holes. These air-holes act like strong barriers, so they are the "wire mesh" of the sieve. The field of the fundamental mode, which fits into the silica core with a single lobe of diameter between zeros slightly equal (or greater) to 2Λ, is the "grain of rice" which cannot escape through the wire mesh. Whereas, the lobe dimensions for the higher-order modes are smaller, so they can slip between the gaps. When the ratio d/Λ, that is the air-filling fraction of the photonic crystal cladding, increases, successive higher-order modes become trapped. A well geometry design of the fiber cross-section thus guarantees that only the fundamental mode is guide.

B. Photonic Band gap Guiding When photonic crystal fiber design is completely different form the traditional ones, which results from the fact that the photonic crystal cladding has greater refractive index than core. They do not relay on TIR for the guidance of photons. In fact, in order to guide light by TIR, it is necessary that the core is surrounded by a lower-index cladding material. But in photonic band gap guiding the core consist of air hole and there are

no suitable low-loss materials with a refractive index lower than air at optical frequencies. Thus, light is guided due to the presence of band gap. We know that the photonic crystal allows only those photons which have band gap greater than that of PCF cladding band gap. So, all those photons with band higher than PCF band gap evanescent in cladding and the rest propagate in air core. The first hollow-core PCF had a simple triangular lattice of air-holes, and the core was formed by removing seven capillaries in the center of the fiber cross-section. In this type light is guided by using the band gap i.e. only a particular portion can enter in cladding and rest reflect back and lost in air or hollow core. When white light is launched into the fiber core, colored modes are transmitted, thus indicating that light guiding exists only in restricted wavelength ranges, which coincide with the photonic band gap.

3.1.3Modes of Operation

Photonic crystal fibers can be divided into two modes of operation, according to their mechanism for confinement. Those with a solid core, or a core with a higher average index than the microstructure cladding, can operate on the same index-guiding principle as conventional optical fiber — however, they can have a much higher effective- refractive index contrast between core and cladding, and therefore can have much stronger confinement for applications in nonlinear optical devices, polarization-maintaining fibers, (or they can also be made with much lower effective index contrast). Alternatively, one can create a "photonic band gap" fiber, in which the light is confined by a photonic band gap created by the microstructure cladding – such a band gap, properly designed, can confine light in a lower-index core and even a hollow (air) core. Band gap fibers with hollow cores can potentially circumvent limits imposed by available materials, for example to create fibers that guide light in wavelengths for which transparent materials are not available (because the light is primarily in the air, not in the solid materials). Another potential advantage of a hollow core is that one can dynamically introduce materials into the core, such as a gas that is to be analyzed for the presence of some substance. PCF can also be modified by coating the holes with sol-gels of similar or different index material to enhance its transmittance of light.

3.2 THz Band and its Application

Terahertz radiation – also known as sub millimeter radiation, terahertz waves, tremendously high frequency [1] (THF), T-rays, T-waves, T-light, T-lux or THz – consists of electromagnetic

waves within the ITU-designated band of frequencies from 0.1 to 30 terahertz (THz) [2]. One terahertz is 1012 Hz or 1000 GHz. Wavelengths of radiation in the terahertz band correspondingly range from 1 mm to 0.1 mm (or 100 μm). Because terahertz radiation begins at a wavelength of one millimeter and proceeds into shorter wavelengths, it is sometimes known as the sub millimeter band and its radiation as sub millimeter waves, especially in astronomy. Terahertz radiation can penetrate thin layers of materials but is blocked by thicker objects. THz beams transmitted through materials can be used for material characterization, layer inspection, and as an alternative to X-rays for producing high resolution images of the interior of solid objects. [3] Terahertz radiation occupies a middle ground between microwaves and infrared light waves known as the "terahertz gap", where technology for its generation and manipulation is in its infancy. It represents the region in the electromagnetic spectrum where the frequency of electromagnetic radiation becomes too high to be measured digitally via electronic counters, so must be measured by proxy using the properties of wavelength and energy. Similarly, the generation and modulation of coherent electromagnetic signals in this frequency range ceases to be possible by the conventional electronic devices used to generate radio waves and microwaves, requiring the development of new devices and techniques. Terahertz radiation falls in between infrared radiation and microwave radiation in the electromagnetic spectrum, and it shares some properties with each of these. Like infrared and microwave radiation, terahertz radiation travels in a line of sight and is non-ionizing. Like microwave radiation, terahertz radiation can penetrate a wide variety of non-conducting materials. Terahertz radiation can pass through clothing, paper, cardboard, wood, masonry, plastic and ceramics. The penetration depth is typically less than that of microwave radiation. Terahertz radiation has limited penetration through fog and clouds and cannot penetrate liquid water or metal. [5] Terahertz radiation is not ionizing yet can penetrate some distance through body tissue, so it is of interest as a replacement for medical X-rays. Due to its longer wavelength, images made using terahertz waves have lower resolution than X-rays and need to be enhanced (see figure at right). [4] The earth's atmosphere is a strong absorber of terahertz radiation, so the range of terahertz radiation in air is limited to tens of meters, making it unsuitable for long-distance communications. However, at distances of ~10 meters the band may still allow many useful applications in imaging and construction of high bandwidth wireless networking systems, especially indoor systems. In addition, producing and detecting coherent terahertz radiation remains technically challenging, though inexpensive commercial sources now

exist in the 0.3–1.0 THz range (the lower part of the spectrum), including gyrotrons, backward wave oscillators, and resonant-tunneling diodes.

3.2.1 Application

Appearance of THz communications brings to life several groups of potential applications. Some of them present the evolution of existing ones, while the others are almost infeasible without the discussed technologies. This section enumerates the major applications and usage scenarios for THz communications and well as briefly mention the motivation for them and the envisioned benefits.

3.2.1.1 Information showers

The inherently small communication range of THz cells inspired the community to search for the scenarios, where small (few meters radius maximum) and extremely high-rate (up to Tbps) cells can be used in the most efficient way. This group of ideas is typically branded as “information shower” or, less frequently, “data shower”. The concept suggests deployment of THz access points (APs) in the areas with high human flow (e.g. gates to the metro station, public building entrances, shopping mall halls, etc.). With such a deployment strategy, each of the passing users is able to receive bulk data (up to several GBs), just while passing this AP. Such information showers can be used do seamlessly deliver software updates as well as other types of heavy traffic, such as high-quality video (e.g. a movie to watch in a train). As the contact time between the user’s terminal is very small (in the order of seconds), the introduction of information showers to the existing networking architecture requires partial redesign of several layers to enable fast nodes association and authentication as well as timely content delivery to the appropriate information shower and caching it there. Meanwhile, it has been recently demonstrated that in certain scenarios introduction of just few THz APs and forwarding all the heavy and delay-tolerant traffic to them whenever possible, allows to substantially off load the macro-scale network [11].

3.2.1.2 Mobile access

The applicability of THz communications to typical usage scenarios (e.g. indoor WLAN access) is limited due to considerable propagation losses. This could be addressed by trading the capacity of THz access points for coverage, primarily by reducing the utilized bandwidth and moving the

entire communications from above 1 THz to the so-called “lower terahertz” carriers around 300 GHz. As a result, it is possible to create reliable wireless links over tens of meters while retaining the capacity of tens of gigabits per second, which makes Wi-Fi-like THz access points (or even femto-cells for cellular access) become feasible. This application is both one of the most desirable ones, but also very challenging due to requirement of reliable beam tracking and effective medium access control.

3.2.1.3 Security-sensitive communications

An ability to create highly directional beams with miniature size antenna arrays in conjunction with the high theoretical capacity of THz links results in a number of benefits for the security-sensitive usage, especially in military applications. The typical military scenario presents a battle field with numerous heterogeneous units (soldiers, armored personnel carriers, tanks, etc.) forming a THz ad hoc network. The primary advantage of the considered technology in comparison to lower frequencies is a physical inability to eavesdrop or even notice the transmission for any node located outside the transmitter beam. Therefore, the security of the transmitted data can be ensured not only by the proper encryption scheme, but also by the geometry of the network itself. The idea of utilizing directional THz antennas to improve the security of the military links has been recently expanded for the civil use as well. Particular use cases range from the ATM with wireless authentication up to the kiosk downloading. The nature of THz links with limited communication range and narrow beams also provides fruitful ground for the physical layer security techniques.

3.3 Conclusion

Photonic crystal fibers (PCFs) are a new class of optical waveguides, which have attracted large scientific and commercial interest during recent years. PCFs are microstructure waveguides, in silica or polymer, with a large number of air holes located in the cladding region of the fiber. In PCFs, light can be guided either by effective index mechanism related to the modified total internal reflection (TIR) or through light confinement by the photonic band gap (PBG) phenomenon. By introducing different gases, liquids or solid materials into the air holes, the propagation parameters of PCF can be finely tuned, providing new functionalities.

Chapter 4

Design methodology and simulations of proposed PCFs

4.1 Hexa Circular Cladding with Circular Core Structure

A noble structure of photonic crystal fiber has been suggested to minimize the effective material loss. The cross-sectional panorama of the proposed design is displayed in Figure 4.1. Five rings are used for hexagon cladding structure. The diameter of each air hole in the cladding is denoted by d. In the cladding the center to center distance between two adjacent circular air holes is denoted by Λ and Λ_1. The distance between two adjacent air holes lies in the same ring are denoted by Λ_1 and that lies in the other ring denoted by Λ. They are connected with each other by $\Lambda_1 = 0.98\ \Lambda$.

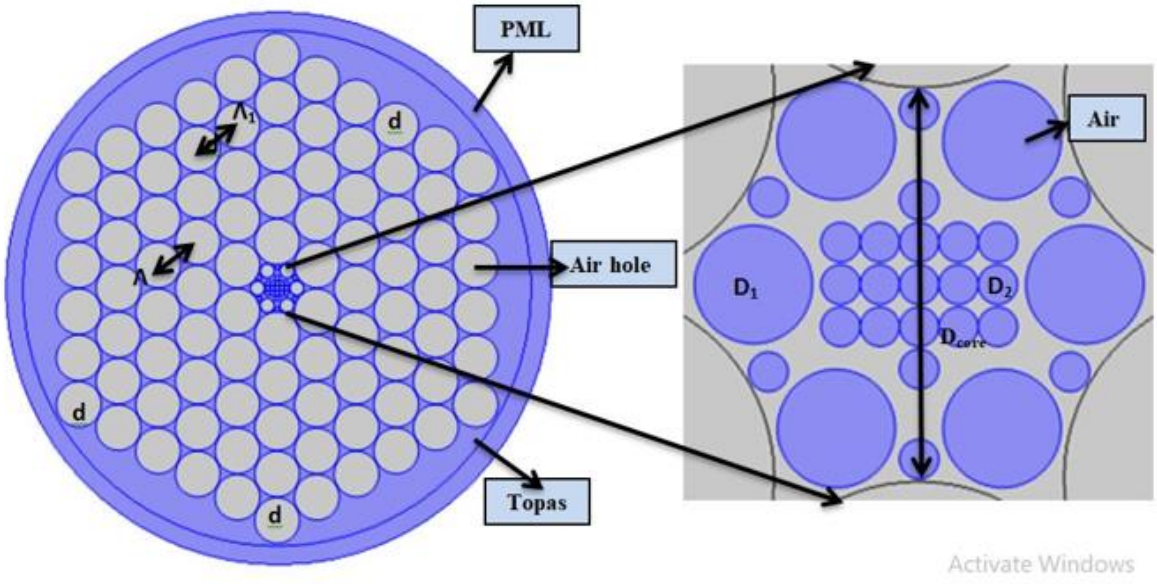

Figure 4.1 Cross sectional view of the proposed hexagon porous-core THz fiber

The diameter of the proposed core structure is demonstrated by D. The core structure of the proposed design is a combination of six large air holes which is denoted by D_1 and 23 small air holes which are denoted by D_2 respectively. The diameter of the D_1 is forty-two times of porosity and the diameter of the D_2 is the fourteen times of porosity. Topaz has been used as a background material of this proposed fiber because it offers superior glass transition temperature than Zeonex and also it has lower bulk material absorption loss than PMMA and Teflon. The

structure of our proposed photonic crystal fiber (PCF) is designed and theoretically investigated using full vector finite element method (FEM) based software COMSOL Multiphysics 5.3 a. To absorb the scattered electromagnetic waves toward the surface, a perfectly matched layer (PML) is used outside the cladding area and the thickness of the PML region used for the calculation is about 7% of the total fiber radius. User controlled mesh size were used for getting the best result in this fiber. The complete mesh of the fiber consists of 81606 element, 7684 boundary elements, 484 vertex elements and the number of degrees of freedom solved for 571691 and the average element quality was 0.4031.

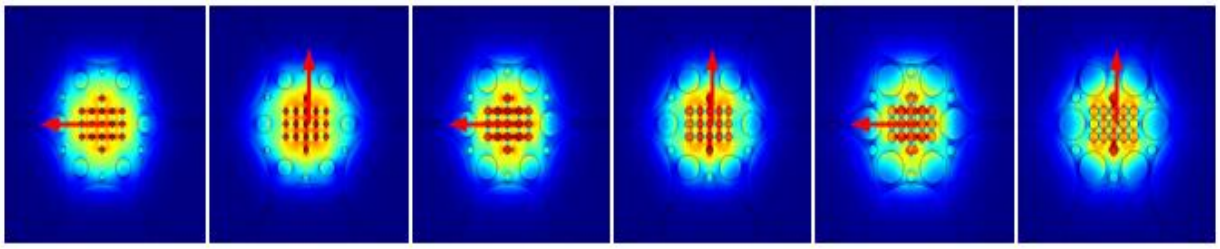

(a) **(b)** **(c)** **(d)** **(e)** **(f)**

Figure 4.2: Mode field profiles of the hexagon cladding with circular core fiber for different porosities.

Figure 4.2 shows the mode field distributions of the proposed PCF for both x-polarization and y-polarization at different core porosities. It is clearly evident from the figure that the mode power is tightly confined within the porous core, which is essential for the transmission of THz waves. As the porosity is increased, the difference in refractive index between the core and the cladding reduces. As a result, the mode field starts to spread out towards the cladding region, which can be observed from the figure.

4.2 Hexa Circular Cladding with Slotted Core Structure

Figure 4.3 depicts the cross-sectional view of the slotted core PCF. As we can see here, the structure has a compact arrangement of circular air holes in the cladding region forming a regular hexagon while in the core; we have rectangular slots of variable lengths. The overall geometry having a diameter of 1633 µm contains 5 layers of circular air holes in the cladding, 13 rectangular slots in the core and we introduce asymmetry in the core intending to achieve ultra-high birefringence. This number is carefully selected to transmit maximum power through the

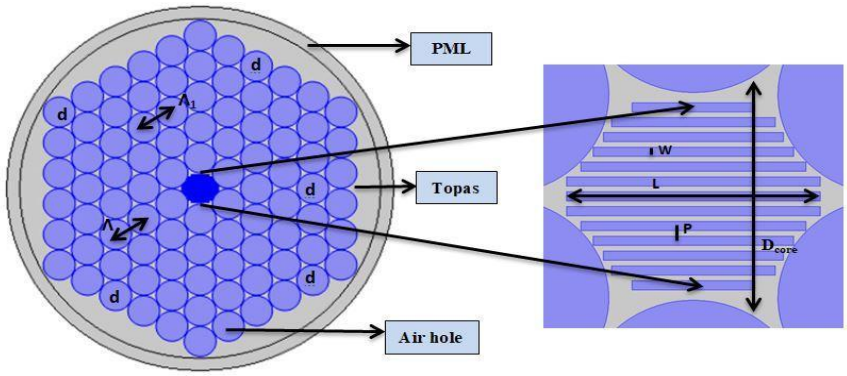

Figure 4.3: Cross-section of the proposed hexagon cladding with slotted-core THz fiber

slots i.e. to improve the core power fraction. Additionally, it allows sufficient separation between two adjacent slots so that overlapping between air slots do not occur. The air holes in the cladding region have a diameter d, the distance between two adjacent air holes in the same layer is denoted by Λ_1 and distance between air holes in the adjacent layer is represented as Λ and relation between them is $\Lambda_1 = 0.98\ \Lambda$. In the core, the center to center distance between two consecutive rectangular slots is denoted by p in the figure, and the value has been set to 10 µm. The maximum length L of the slot is chosen to be in the middle, and gradually it reduces to the minimum length in the outermost slot. And the width of each slot in the core is represented by W. The width has been chosen tactically so that we can control the porosity of the material. The ratio of the area of all the slots to the overall area of the core is defined as porosity. The length of three slots in the center is L and is equal to 310 µm. Now the length of the successive slots on both sides is 275 µm, 240 µm, 220 µm, 200 µm, and 150 µm. In figure 4.4, one-fourth of the total mesh of our design is shown. For our design, the complete mesh of the fiber consists of 14008 elements, 2122 boundary elements, and 76 vertex elements, and the number of degrees of freedom solved for is 98277. Finer mesh analysis is employed here to find these values. The minimum element quality of about 0.4569 is obtained from this mesh analysis. An artificial absorbing layer, known as the perfectly matched layer (PML) is imposed on the outer cladding in order to limit the computational domain, to provide anti-reflectivity, to absorb the electromagnetic field propagating towards the surface and to calculate the confinement loss. During the simulation, the PML thickness of the fiber was optimized first by running several subsequent simulations. The optimized thickness was kept 7% of the total radius of the fiber in the rest of the study.

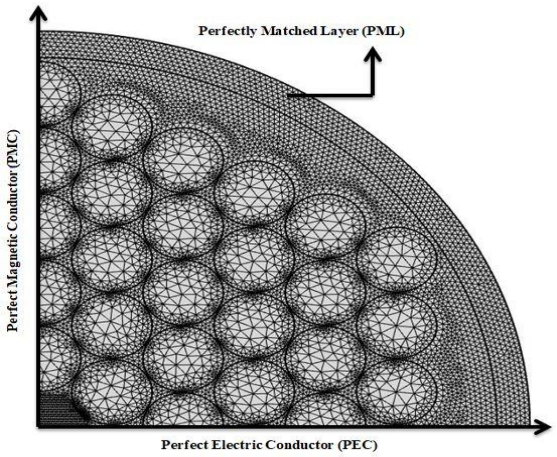

Figure 4.4: Mesh of the proposed hexagon cladding with slotted-core design

We have chosen TOPAS (the trade name of Cyclic Olefin Copolymers) as the host material of our PCF for its excellent innate characteristics. It has a constant refractive index of 1.53 in the range of 0.1 - 2.0 THz [41], negligible bulk material absorption loss (0.2 cm^{-1} at f = 1 THz) [21], insensitivity to humidity [56], the fact that it's suitable for bio-sensing and research [57].

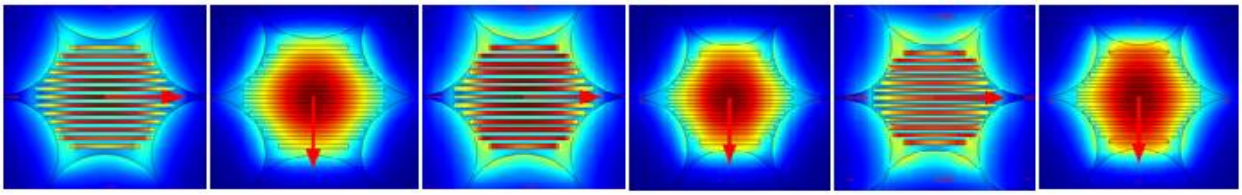

Figure 4.5. Mode field profiles of the proposed for hexagon cladding with slotted-core

Moreover, it shows low dispersion, low confinement loss, and proper protection against water vapor absorption [21]. For efficient transmission of the THz wave, the electromagnetic field should be tightly confined in the core region. The fundamental mode field profiles of the proposed PCF for the two orthogonal polarization components at 70%, 80% and 90% core porosities are shown in figure 4.5. The following figure unveils that the light is confined tightly in the core region. It is unquestionably evident from the above figure that increasing the core porosity results in the spreading of mode power towards the cladding region. Since the increment

of core porosity causes the reduction of index contrast between core and cladding, the guiding modes tend to spread into the cladding region.

4.4 Octa square cladding with slotted core structure

The cross section region of this proposed photonic crystal fiber is shown in Figure 4.6. In this figure, the complete cross section of the proposed porous-core THz fiber is shown with an enlarged view of the porous core. The structure of the PCF is designed by using commercially available software COMSOL 5.3a. TOPAS is used as a background material of this proposed fiber and air is used as a material of the core and cladding region. We have proposed an octagonal shaped cladding region to fortify low effective material loss, high core power fraction along with flatten dispersion properties. Many shapes have been assessed before but the structure we are examining here gives more precise and satisfactory result than the previously discussed ones. This PCF's cladding region is modeled as an octagonal form composed of a mixture of octagonal and square air holes. Four square buildings surround one octagonal structure in the cladding. The key region is the structure of slotted air holes in the core. The slotted structure plays a vital role in enriching the confinement and subsequently minimizing the EML. The PML (perfectly matched layer) is appointed through the outer circle in the structure. PML is used to

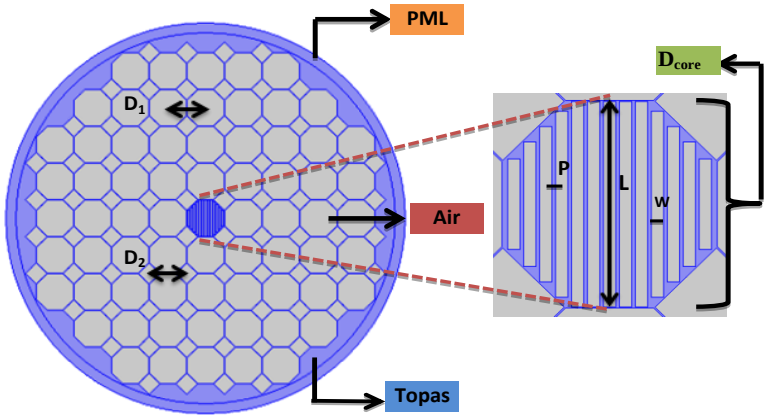

Figure 4.6: Cross section of the proposed for Octa square cladding with porous-core THz fiber

Protect light against reflection and simulation requires it. But practical characterization requires no assistance of PML. The PML thickness is kept at 5 percent of the complete radius of fiber. User-controlled mesh size has been used in this fiber design to achieve more accurate outcome. The fiber's full mesh consists of 294062 element, 31632 boundary elements, 908 vertex elements

and the number of degrees of freedom solved for is 34224 and the average element quality was 0.4156. The distance between two octagon and square structure in cladding region are denoted by D_1 and D_2 respectively. The core diameter of the proposed structure is defined by D. octagonal shape core consists of fourteen rectangular slots, where W is the width of each rectangular slot and L is the length of each rectangular slot. The length of the rectangular slots of the core of this proposed fiber is shortening gradually even though they all bear the same width. The length of the all slots in the core is kept fixed. We varied only the width and the width is varied by varying the core diameter and core porosity which is formed by the following equation given bellow

$$W = porosity \times 0.647072952 \times \pi \times (D/2)^2 / (L + L_1 + L_2 + L_3 + L_4) \ ,$$

Where, L is the length of the center rectangular slot of the core. The lengths of the five center rectangular slots (2 on the left of the center one, 2 on the right of the center one and the center one) are same and L_1, L_2, L_3, L_4 represents the other slots from the center respectively. Each slot is separated from other slot by 0.097*p which contributes for keeping the slot free from overlapping. The dimensions of L are 368 um, L_1 is 333 um, L_2 is 278 um, L_3 is 223 um, and L_4 is 162 um respectively. Pitch is defined by the distance of center to center from one slot to other. This is denoted by P. The distance between two centers of the core slot has been set at a value 28 µm.

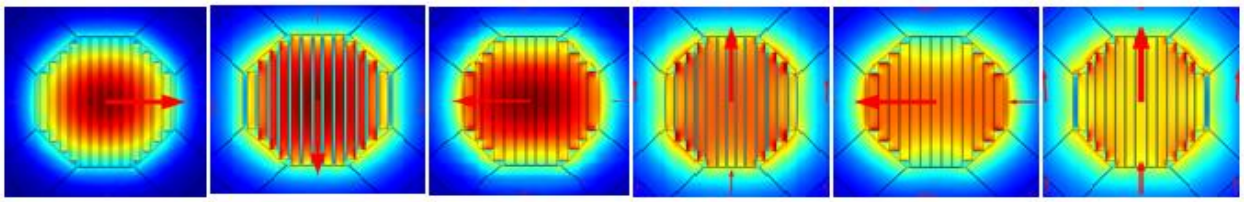

(a) (b) (c) (d) (e) (f)

Figure 4.7. Mode field profiles of the proposed fiber for Octa square cladding with porous-core.

Figure 4.7 shows the mode field distributions of the proposed design for both x- and y-polarizations at different core porosities. It is clearly apparent from the figure that the mode power is firmly confined within the porous core, which is essential for the transmission of THz waves. As the porosity is augmented, the difference in refractive index between the core and the

cladding reduces. As a result, the mode field starts to spread out in the direction of the cladding region.

4.5 Octa circular cladding with slotted core structure

We proposed another novel structure of PCF for reduce the effective material loss and to flatten the dispersion properties respectively. Based on the Finite Element Method (FEM), commercially available software COMSOL Multiphysics 5.3 a has been used to design and generate results.

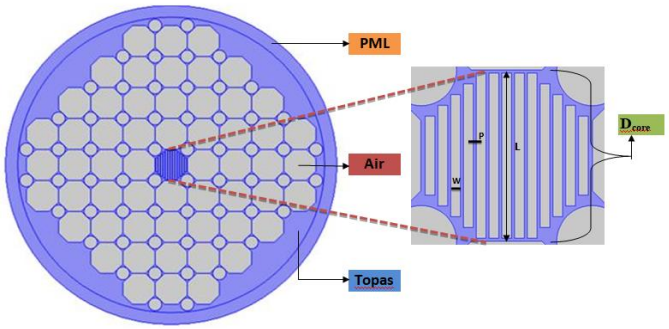

Figure 4.8: Cross section of the proposed Octa circular cladding with porous-core THz fiber.

The schematic diagram of the proposed design is shown in Figure 4.8 with extended view of the porous core. Here the cladding structure is framed by customary octagon shaped air gap and circular air gap. It is designed in such a way, that every octagon is fastened by round about air gap. The octagonal shaped core is formed by thirteen rectangular air slots. The core diameter is defined by D. L is the length and W is the width of the slotted core. The distance from center to center from one slot to other slot is called pitch. This is denoted by P that has the value of 10µm. The dimension of the slotted core length is decreasing gradually except the five center slots. Only the width, W is varied by altering the core diameter, D and core porosity according to this following equation

$$W = porosity \times 0.647072952 \times \pi \times \left(D/2\right)^2 / \left(L + L_1 + L_2 + L_3 + L_4\right)$$

Here L is the length of the five center slots and the decreasing slots are denoted by L_1, L_2, L_3 and L_4 respectively. The dimensions of L, L_1, L_2, L_3 and L_4 are 310 µm, 275 µm, 240 µm, 220 µm and 200 µm respectively. To avoid overlapping, each slot is separated by 0.097×P from other neighbor slots. In order to get utmost precision in the simulation, user controlled mesh size is

selected. The complete mesh of the fiber consists of 10,804 boundary elements, 652 vertex elements and the number of degrees of freedom solved for 702,958 and the average element quality is 0.93 and this indicates the computational error is less than 1%. The outer part of the PCF is surrounded by a perfectly matched layer (PML) boundary condition. This PML boundary condition protects the PCF from the effect of surrounding environment and also acts as an anti-reflective layer [29]. The PML of this proposed fiber is 9% of the total radius of the fiber. Nevertheless, this PML boundary condition is used only for simulation purposes but in practical characterization of PCF, perfectly matched layer condition does not carry any significance.

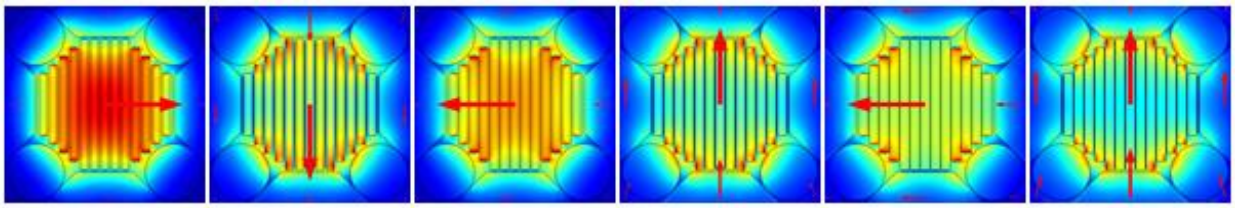

(a) (b) (c) (d) (e) (f)

Figure 4.9. Mode field profiles of the proposed fiber for octa circular cladding with slotted core

Figure 4.9 shows the mode field distributions of the proposed PCF for both x- and y-polarizations at different core porosities. It is clearly evident from the figure that the mode power is tightly confined within the porous core, which is essential for the transmission of THz waves. As the porosity is increased, the difference in refractive index between the core and the cladding reduces. As a result, the mode field starts to spread out towards the cladding region, which can be observed from the figure.

4.6 Conclusion

We investigated an octagonal and hexagonal shaped porous core PCF for Terahertz applications and analyzed numerically with respect to frequency, core diameter and core porosity. An octagonal shaped cladding region is used to ensure low effective material loss, high core power fraction along with flattened dispersion properties. A slotted core PCF is designed here, and its key feature is ultra-high birefringence and very low EML. Moreover, an adequate amount of modal power is transmitted through the core that results in high core power fraction, and the compact arrangement of air holes in the cladding helps to maintain low confinement loss.

Chapter 5

Different Factors and Results of proposed PCFs

The main aim in the design of PC-PCFs for THz wave guiding is to maximize modal confinement and reduce the material absorption loss of the fiber. To achieve this aim, the key design parameters must be carefully selected so that the MTIR can be assured throughout the transmission process. The region under which the fiber obeys the single mode property in terms of both core sizes and pumping frequencies is also theoretically characterized. Another important optical loss that needs investigation is bending loss at small bending since high bending losses may cause the light to radiate out of the core, which amounts to degradation of light intensity at the receiver end.

5.1 Single mode fiber

In fiber-optic communication, a single-mode optical fiber (SMF) is an optical fiber designed to carry light only directly down the fiber - the transverse mode. Modes are the possible solutions of the Helmholtz equation for waves, which is obtained by combining Maxwell's equations and the boundary conditions. These modes define the way the wave travels through space, i.e. how the wave is distributed in space. Waves can have the same mode but have different frequencies. This is the case in single-mode fibers, where we can have waves with different frequencies, but of the same mode, which means that they are distributed in space in the same way, and that gives us a single ray of light. Although the ray travels parallel to the length of the fiber, it is often called transverse mode since its electromagnetic vibrations occur perpendicular (transverse) to the length of the fiber. The 2009 Nobel Prize in Physics was awarded to Charles K. Kao for his theoretical work on the single-mode optical fiber.

5.1.1 Characteristics

Like multi-mode optical fibers, single mode fibers do exhibit modal dispersion resulting from multiple spatial modes but with narrower modal dispersion. Single mode fibers are therefore better at retaining the fidelity of each light pulse over longer distances than multi-mode fibers. For these reasons, single-mode fibers can have a higher Band width than multi-mode fibers. Equipment for single mode fiber is more expensive than equipment for multimode optical fiber, but the single mode fiber itself is usually cheaper in bulk. A typical single mode optical fiber has

a core diameter between 8 and 10.5 µm and a cladding diameter of 125 µm. There are a number of special types of single-mode optical fiber which have been chemically or physically altered to give special properties, such as dispersion-shifted fiber and nonzero dispersion-shifted fiber. Data rates are limited by polarization mode dispersion and chromatic dispersion. As of 2005, data rates of up to 10 gigabits per second were possible at distances of over 80 km (50 mi) with commercially available transceivers (Xenpak). By using optical amplifiers and dispersion-compensating devices, state-of-the-art DWDM optical systems can span thousands of kilometers at 10 Gbit/s, and several hundred kilometers at 40 Gbit/s. The lowest-order bounds mode is ascertained for the wavelength of interest by solving Maxwell's equations for the boundary conditions imposed by the fiber, which are determined by the core diameter and the refractive indices of the core and cladding. The solution of Maxwell's equations for the lowest order bound mode will permit a pair of orthogonally polarized fields in the fiber, and this is the usual case in a communication fiber. In step-index guides represent by equation 5.1[30].

$$V = \frac{2\pi rf}{c}\sqrt{(n_{co}^2 - n_{cl}^2)} \leq 2.405 \qquad 5.1$$

η_{co} Represents the refractive index of the core region and η_{cl} represents the refractive index of the cladding region, f is denoted by operating frequency and c is the speed of light in free space. V-parameter value of a fiber determines whether the fiber is single mode or multi-mode. A fiber can be single mode when its V-parameter value less or equal 2.405.

5.1.2 Normalized frequency of Octa square cladding with slotted core design.

Figure 5.1 and Figure 5.2 depict the ability of our proposed photonic crystal fiber to operate in single mode condition. Our proposed fiber operates as single mode operation as V remains less than the reference value. After further analysis, we can perceive that V-parameter decreases with the increase of porosity since with the increase of porosity, refractive indices become lower. Referring to the equation of determining V-parameter, we can assess that refractive index has an inverse correspondence to V-parameter value and so does Porosity.

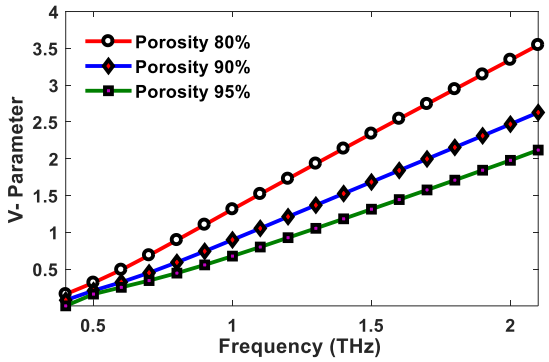

Figure 5.1: V-parameter vs frequency for Octa square design

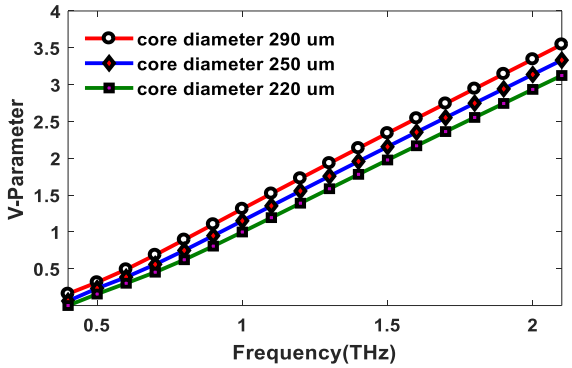

Figure 5.2: V-parameter vs frequency for Octa square design

The reverse case is observed in case of V-parameter being reduced. From the figure above, we can assess that V-parameter has a direct correspondence to core diameter. It can also be confirmed that the single mode operation of our proposed THz fiber occurred at 80% porosity when core diameter was 280 um and frequency was less than 1.6 THz.

5.1.3 Normalized frequency of hexagon cladding with slotted core design

Figure 5.3 demonstrates the behavior of the V-parameter for different porosities over the frequency range of 0.5–1.6 THz. It can be noted from figure 5.3 that with increasing frequency, the value of the V parameter increases. It is due to the reason that, increase in frequency causes a significant increase of index contrast between effective indices of core and cladding. Therefore V parameter increases. Figure 5.3 also depicts that the value of normalized frequency is reduced

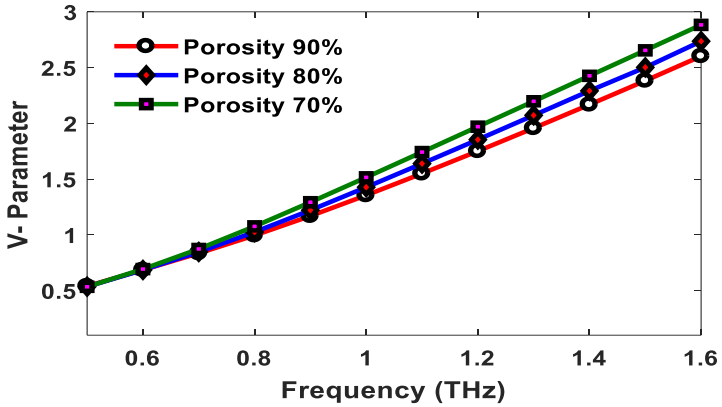

Figure 5.3. V-parameter vs frequency at different porosities for hexagon cladding with slotted core design.

with an increment of the core porosity. When the core porosity is increased, the index difference between core and cladding reduces, which in terms decreases the value of the V parameter. It is nicely visualized from figure 5.3 that the value of the V-parameter for our proposed design remains under 2.405 between frequency ranges 0.5-1.3 THz. So our proposed fiber is a single-mode fiber, which enhances the long-distance communication applications.

5.1.4 Normalized frequency of hexagon cladding with circular core design.

It can be seen from Figure 5.4 that our proposed fiber operates as single mode operation because of the value of v parameter is less than reference value. It can be confirmed that the single mode operation of our proposed THz fiber at 90% porosity when core diameter 280 µm and frequency less than 1.5 THz.

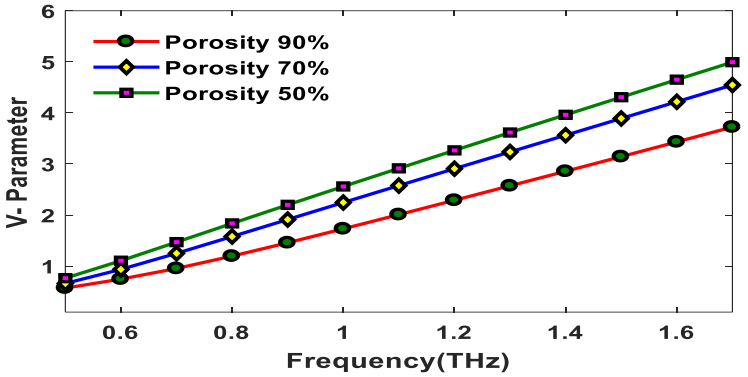

Figure 5.4: V-parameter vs frequency at different core porosities for hexagon cladding with circular core design.

5.1.5 Normalized frequency of Octa circular cladding with slotted core design.

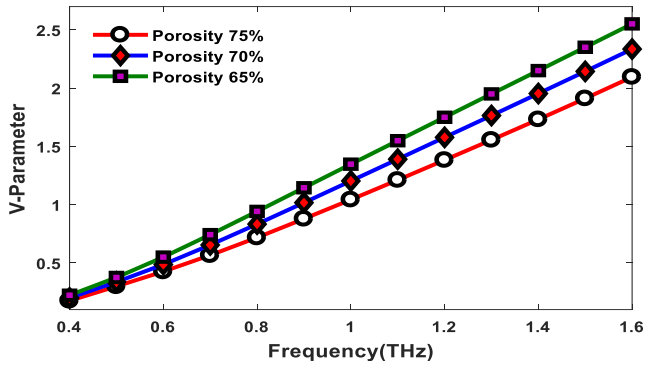

Figure 5.5: V-parameter versus frequency at three different porosities for Octa circular cladding with slotted core design

From Figure 5.5, it is observed that the proposed fiber operates in the single mode operation because the value of v parameter does not exceed 2.405. Moreover the value of v-parameter decreases with the increase in porosity.

5.2 Multi-mode fiber

Multi-mode optical fiber is a type of optical fiber mostly used for communication over short distances, such as within a building or on a campus. Typical multimode links have data rates of 10 Mbit/s to 10 Gbit/s over link lengths of up to 600 meters (2000 feet).

5.2.1 Applications

The equipment used for communications over multi-mode optical fiber is less expensive than that for single-mode optical fiber. Typical transmission speed and distance limits are 100 Mbit/s for distances up to 2 km (100BASE-FX), 1 Gbit/s up to 1000 m, and 10 Gbit/s up to 550 m. Because of its high capacity and reliability, multi-mode optical fiber generally is used for backbone applications in buildings. An increasing number of users are taking the benefits of fiber closer to the user by running fiber to the desktop or to the zone. Standards-compliant architectures such as Centralized Cabling and fiber to the telecom enclosure offer users the ability to leverage the distance capabilities of fiber by centralizing electronics in telecommunications rooms, rather than having active electronics on each floor.

5.2.2 Comparison with single-mode fiber

The main difference between multi-mode and single-mode optical fiber is that the former has much larger core diameter, typically 50–100 micrometers; much larger than the wavelength of the light carried in it. Because of the large core and also the possibility of large numerical aperture, multi-mode fiber has higher "light-gathering" capacity than single-mode fiber. In practical terms, the larger core size simplifies connections and also allows the use of lower-cost electronics such as light-emitting diodes (LEDs) and vertical-cavity surface-emitting lasers (VCSELs) which operate at the 850 nm and 1300 nm wavelength (single-mode fibers used in telecommunications typically operate at 1310 or 1550 nm). However, compared to single-mode fibers, the multi-mode fiber bandwidth–distance product limit is lower. Because multi-mode fiber has a larger core- size than single-mode fiber, it supports more than one propagation mode; hence it is limited by modal dispersion, while single mode is not. The LED light sources sometimes used with multi-mode fiber produce a range of wavelengths and these each propagate

at different speeds. This chromatic dispersion is another limit to the useful length for multi-mode fiber optic cable. In contrast, the lasers used to drive single-mode fibers produce coherent light of a single wavelength. Due to the modal dispersion, multi-mode fiber has higher pulse spreading rates than single mode fiber, limiting multi-mode fiber‘s information transmission capacity. Single-mode fibers are often used in high-precision scientific research because restricting the light to only one propagation mode allows it to be focused to an intense, diffraction-limited Spot. Jacket color is sometimes used to distinguish multi-mode cables from single-mode ones. The standard TIA-598C recommends, for non-military applications, the use of a yellow jacket for single-mode fiber, and orange or aqua for multi-mode fiber, depending on type. Some vendors use violet to distinguish higher performance OM4 communications fiber from other types.

5.3 Material absorption loss

Absorption of signal is a serious loss mechanism in an optical fiber. Absorption occurs in optical fibers due to the presence of imperfections in the atomic structure of the fiber material, due to some basic inherent intrinsic material properties and due to some extrinsic material properties. Imperfections may appear in atomic structure due to oxygen deficiencies and missing of certain molecules. Diffusion of hydrogen molecules may also induce absorption. But the contribution from imperfections is relatively small in fiber optic absorption losses. Inherent intrinsic absorption is caused by basic fiber material properties. If a material is free from impurities and imperfections, then entire absorption is due to intrinsic absorption. Silica fibers possess very low intrinsic material absorption. Here absorption is caused by the vibration of silicon-oxygen bonds. The interaction between these bonds and the electromagnetic field of the optical signal is responsible for intrinsic absorption. Presence of impurities in the fiber material leads to extrinsic absorption. This is caused by the electronic transition of metal impurity ions from one energy level to another. Another reason for extrinsic absorption is the presence of hydroxyl ions in the fiber. Effective material loss represent by equation 5.2, [30].

$$\alpha_{eff} = \sqrt{\frac{\varepsilon_0}{\mu_0}} \left(\frac{\int_{mat} n_{mat} |E|^2 \alpha_{mat} dA}{\left| \int_{all} S_z dA \right|} \right) \qquad 5.2$$

Where, ε_0 and μ_0 are considered to be the relative permittivity and permeability in vacuum respectively, n_{mat} is the refractive index of Topas,α_{mat} is the bulk material absorption loss, **E** is

the modal electric field and S_z is the z component of the pointing vector (S_z = ½(**E** × **H***).z),where **E** and **H** are the electric and magnetic fields respectively.Fig.5 depicts the characteristics of EML as a function of core diameter with different core porosities. From where it is observed that, for the same porosity values there is a significant change of EML when the core diameter changes. It is a loss mechanism related to the material composition and fabrication process of the fiber which results in the dissipation of some of the transmitted optical power as heat in waveguide. The absorption of light may be intrinsic (caused by one or more major components of glass) or extrinsic (caused by impurities within the glass).

5.3.1 Material absorption loss of Octa square cladding with slotted core design.

EML increases proportionally with frequency and inversely with core porosity. This occurrence is related to the number of air holes being used in the designed fiber. As the number of air holes increases, less amount of material has to interact with light. This results in minimization of α_{mat} (Bulk material absorption loss) and eventually reduction of EML occurs (refer to the above equation). This concludes that at increasing porosity, we will have minimized EML. This conjecture is confirmed by Figure 5.6 demonstrating the variation of effective material loss as a function of frequency for different porosity. Again, when the core diameter increases, the confinement becomes loose at the core or at the center. Thus interaction of light with material increases which in result increases the EML.

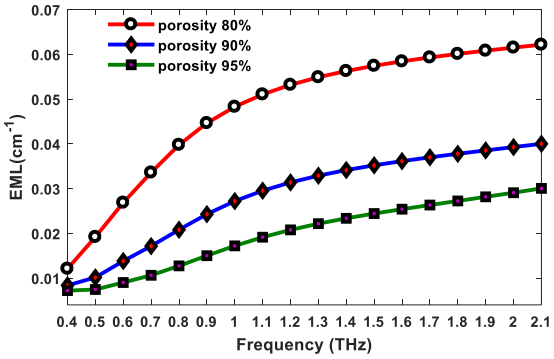

Figure 5.6: Effective material loss vs frequency at different core diameters for Octa square design

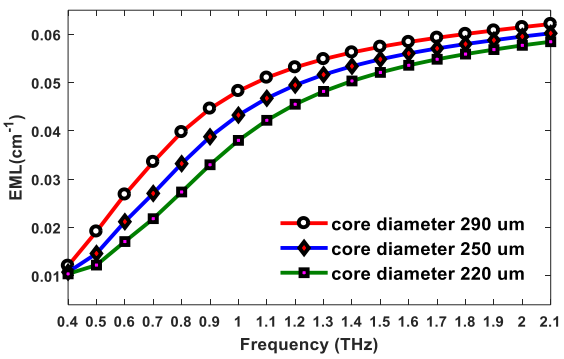

Figure 5.7: Effective material loss vs frequency at different core porosities for Octa square design

This is demonstrated by Figure 5.7 where variation of effective material loss as a function of frequency for different diameter is indicated. At higher frequency light is well confined and therefore it contacts with more TOPAS material which leads to increase the effective material

loss. From both figures we can deduce that the curve shows a positive increment with increasing frequency. These results are in accordance with our expectations; because according to the empirical equation of calculating material absorption loss, EML depends on frequency [44]. The minimum obtained EML from our proposed photonic crystal is 0.007 cm^{-1}, which is better than previously reported THz photonic crystal fiber [5].

5.3.2 Material absorption loss of hexagon cladding with slotted core design.

We calculated the effective material loss of the proposed fiber as a function of frequency, which is shown in figure 5.8. It is gingerly visualized that the EML is proportional to the frequency, which means that the EML increases with frequency. This can be explained by the fact that stronger confinement occurs for smaller wavelengths and that the core contains a slightly larger

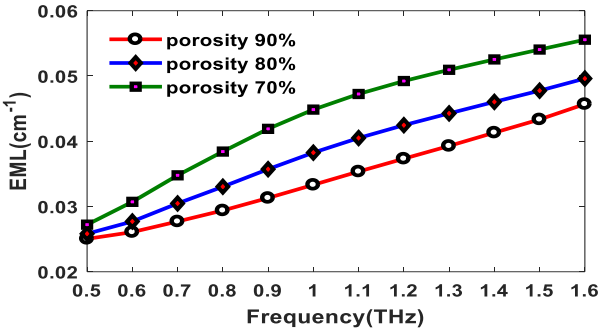

Figure 5.8. Effective Material Loss vs frequency at different porosities for hexagon cladding with slotted core design

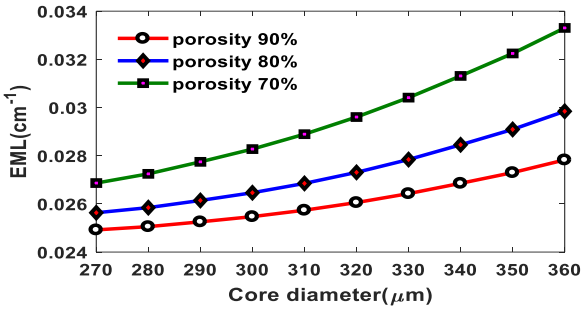

Figure 5.9. Effective Material Loss vs core diameter at different porosities for hexagon cladding with slotted core design

percentage of the bulk material. It is also evident from figure 5.8 that at a fixed frequency, EML can be reduced by using higher core porosities. Higher porosity assists in reducing the EML because higher porosity ensures less material inside the core region. Thus the guiding electromagnetic wave interacts with less amount of material. Therefore, the EML of the proposed PCF decreases. Figure 5.9 reveals the EML property of the proposed waveguide with respect to the fiber geometry. EML as a function of core diameter for three different core porosities (70%, 80%, and 90%) is illustrated in Figure 5.9. It can be seen from the figure that at a fixed core diameter, the value of EML can be reduced by using higher core porosities. The physical explanation behind this Phenomenon was given earlier. On the Other hand, this figure also indicates that for particular core porosity, the EML increases with the increase of core length because the increased core length increases the effective solid material in the core, therefore,

EML increases. So the EML for the proposed design at optimum condition is 0.025, and it is lower than earlier reported THz fibers [1, 13, 14, 58, 64, 68-70].

5.3.3 Material absorption loss of hexagon cladding with circular core design.

Effective material loss is proportional to electromagnetic wave frequency thus it changes significantly with addition in frequency. From Figure 5.10 we can see that increase in frequency increases EML. On the contrary, Figure 5.11 represents decreasing EML when core porosity and core diameter are increased. The reason is, at higher core porosity, a portion of background material is diminished and the mode power streams to a greater extent through the circular air slots creating reduction in EML.

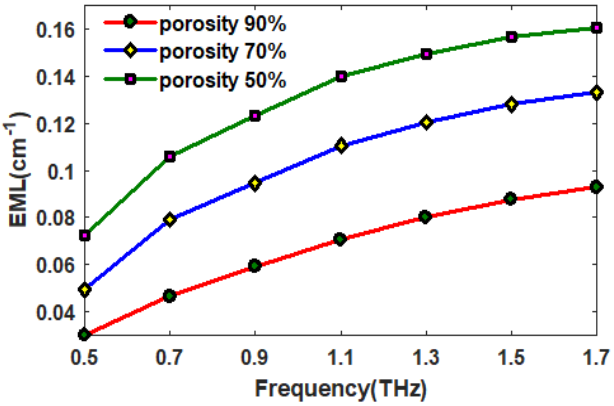

Figure 5.10: Effective material loss vs frequency at different core porosities for hexagon cladding with circular core design.

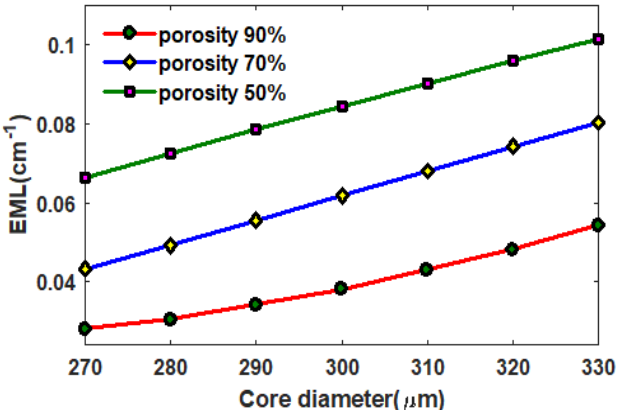

Figure 5.11: Effective material loss vs core diameter at different core porosities for hexagon cladding with circular core design.

Likewise, when the core diameter is expanded light gets less in contact with the material hence bulk absorption loss decreases. Simulation result shows that at 290 μm core diameter, with a high porosity of 90%, the proposed fiber demonstrates an ultra-low effective material loss value of 0.029 cm^{-1}.

5.3.4 Material absorption loss of Octa circular cladding with slotted core design.

From Figure 5.12 we can see, EML increases constantly with frequency [30]. On the contrary, in Figure 5.13 we can see EML is decreasing with both core diameter and core porosity. Core diameter causes the electromagnetic field to experience a greater amount of the solid material, which builds the EML. Effective material loss depends on frequency which is exhibited by the following empirical formula [31] $\alpha(v) = v^2 + 0.63v - 0.13[dB/cm]$..

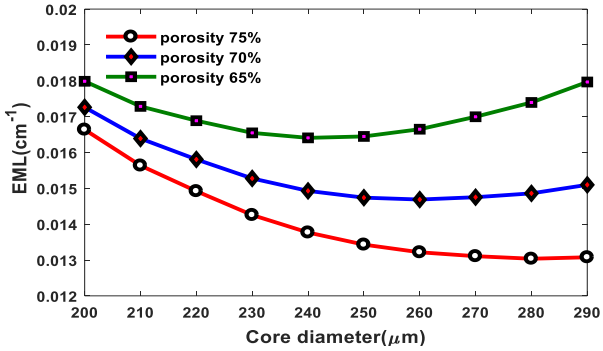

Figure 5.13: Effective material loss (EML) versus frequency at different porosities for Octa circular cladding with slotted core design

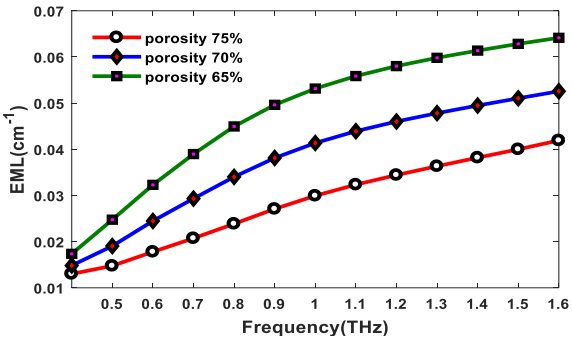

Figure 5.12: Effective material loss (EML) versus core diameter at different porosities for Octa circular cladding with slotted core design

Where, v is the normalized frequency. From Figure 5.12 and Figure 5.13 at 75% porosities we found an optimum value of EML 0.013cm^{-1} at 0.4 THz frequency and 280 µm core diameter.

5.4 Mode power propagation

The amount of useful power propagating through different regions of the fiber also known as core power fraction can be calculated by equation 5.3, [32].

$$\eta = \frac{\int_{X} S_z dA}{\int_{All} S_z dA} \qquad 5.3$$

Where η represents mode power fraction and X represents the area of interests. To design a standard PCF, it is necessary to pass most of the useful power through the core air holes. Higher D_{core} increases the core power fraction but this also increases the EML. On the other hand, as the D_{core} decreases EML also decreases but this also decreases the core power fraction. These are contradictory conditions and needs to select an optimum condition of higher core power fraction and lower EML. At different core porosities, the characteristics of core power fraction as a function of core diameter where it can be observed that amount of core power increases with the increase of core diameter.

5.4.1 Mode power propagation of Octa square cladding with slotted core design.

Core power fraction is an important parameter for designing a THz photonic crystal fiber. Core power fraction is defined as power propagating through air hole in the core.

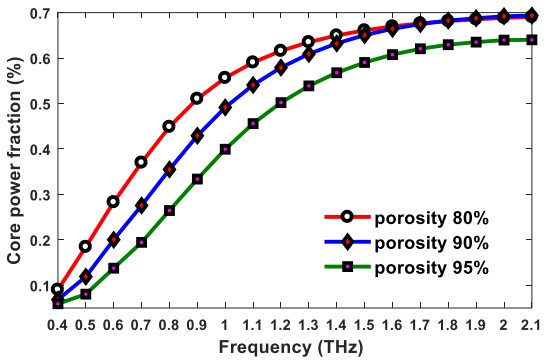

Figure 5.14: Core power fraction vs frequency at different core porosities for Octa square with slotted core design.

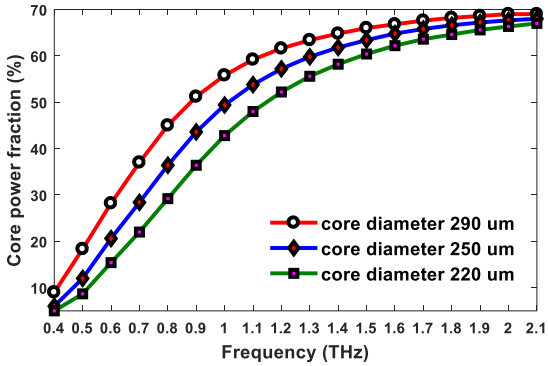

Figure 5.15: Core power fraction vs frequency at different core diameters for Octa square cladding with slotted core design.

Change in core power with respect to frequency for different core porosities and for different core diameters. At higher frequency, light is tightly confined in the core which results in increased ratio of confined area to the total area of the fiber. This phenomenon has been observed in Figure 5.14 and Figure 5.15 as well, where we see core power increases as frequency is increased. It is further perceived that the core power fraction increases with the decrement of core porosity. At higher core porosity light waves are poorly confined in the core and tend to decrease the core power fraction. The opposite case is observed in case of core diameter. Core power fraction seems to increase for increased value of core diameter. Since at higher core diameter, core power fraction is higher as the amount of material used in core increases with core diameter. This information tells us that core power fraction has direct proportional correspondence with frequency, core diameter and inverse correspondence with porosity [44]. Our proposed photonic crystal fiber has a core power fraction of 70% for 290 µm core diameter with a core porosity of 80% which surpasses the earlier reported THz crystal fiber [7].

5.4.2 Mode power propagation of hexagon cladding with slotted core design.

Power fraction in air-core refers to the amount of total mode power that propagates through the air holes of the slotted core. To obtain an ultra-high birefringence and simultaneously avoid the effects of material absorption in the THz region, the majority of power should be concentrated in core air holes. Behaviors of mode power fraction of the proposed design at 70%, 80% and 90%

porosities as a function of frequency are shown in figure 5.16 where we can see that core power fraction is higher for high frequencies and lower for low frequencies. It is evident from figure 8 that at a fixed frequency, power fraction in core air holes decreases when the core porosity is scaled up. The reason is that increasing the value of core porosity leads to an increase in the amount of air volume in the slotted-core region. At a higher porosity, the mode field is delocalized from the core and spread into the cladding, which results in reduced core power fraction. It is possible to increase power fraction in air-slots by decreasing the porosity further. However, that would incur additional EML. Figure 5.17 shows the mutation of core power fraction as a function of core diameter.

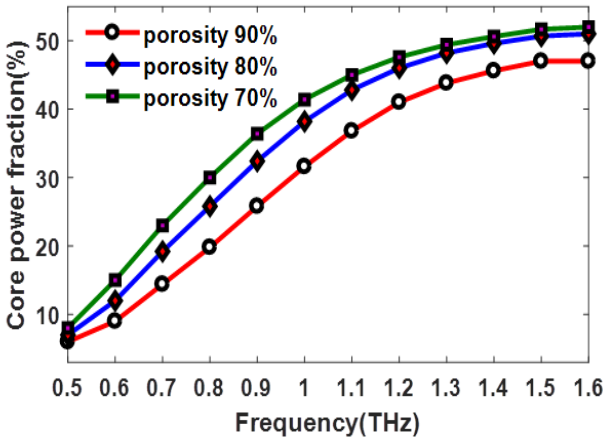

Figure 5.17.Core power fraction vs core diameter at different porosities for hexagon cladding with slotted core design.

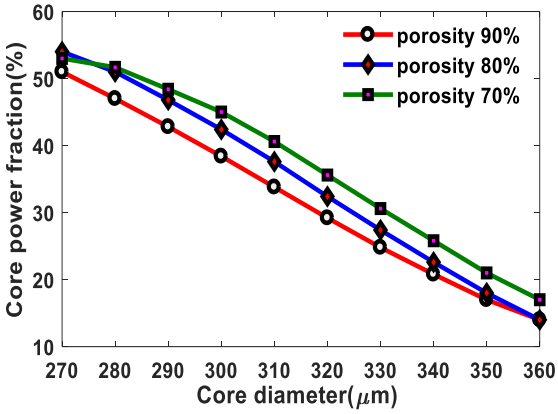

Figure 5.16.Core power fraction vs frequency at different porosities for hexagon cladding with slotted core design.

From figure 5.17 we can see that core power fraction decreases with increasing core diameter. Such an incident happens because the light wave is not confined well at higher core diameter. Thus less amount of power propagates through the core, and as a result, the core power fraction decreases. The core power fraction of our proposed design is 52% at 70% porosity and core diameter 270 μm and to the best of our knowledge, this result is better than previously reported [1, 12, 14, 62, 68, 71-72] THz photonic crystal fibers.

5.4.3 Mode power propagation of Octa circular cladding with slotted core design.

From Figure 5.18 we can see at 65% and 70% core porosity, the core power fraction increments with core diameter, yet remains practically level for 75% porosity. By expanding the core

diameter, the absolute volume of air contrasted with the solid material in the core is expanded, which increases the power fraction. At fixed diameter and frequency, the power fraction increases with core porosity which increases the amount of air inside the core. Thus higher Amount of mode power flows through the core air slots. From Figure 5.19 it is seen core power fraction increases with frequency. However, at exceptionally low frequencies of around 1 THz, the core power fraction is practically comparable for 65% and 70% porosity. Because under low frequency conditions, the confinement of light in the core is low, and subsequently there is

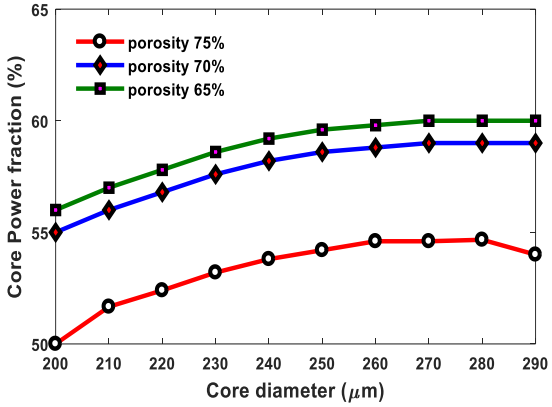

Figure 5.18: Core power fraction versus core diameter at different porosities for Octa circular cladding with slotted core design.

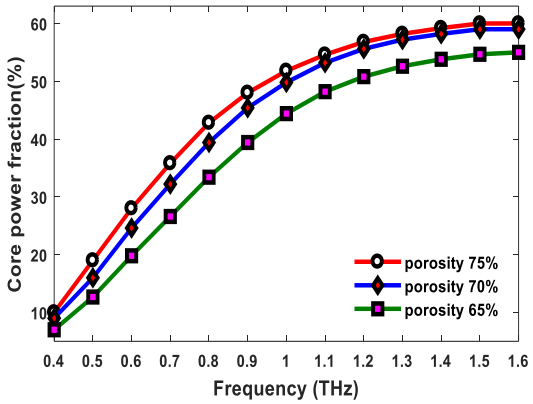

/Figure 5.19: Core power fraction versus frequency at different porosities for Octa circular cladding with slotted core design.

In significant difference between the core power fractions at these two porosities. Finally, maximum core power fraction of 60% is obtained at 65% porosity.

5.4.4 Mode power propagation of hexagon cladding with circular core design.

Figure 5.20 displays at 90% and 70% porosity where core power fraction increases with

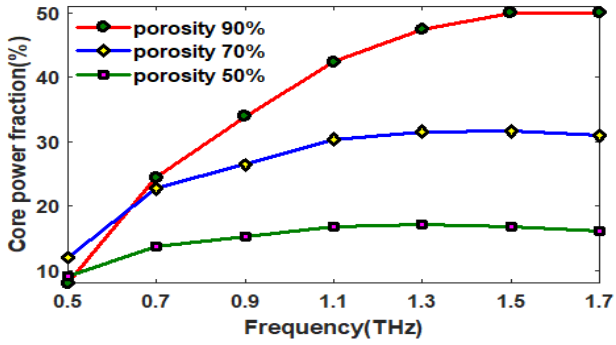

Figure 5.20: Core power fraction vs frequency at different core porosities for hexagon cladding with circular core design.

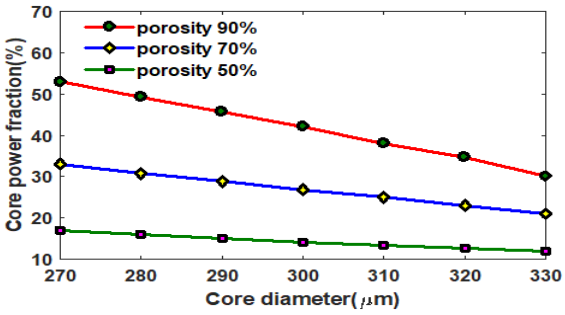

Figure 5.21: Core power fraction vs core diameter at different core porosities for hexagon cladding with circular core design

frequency. But for 50% porosity increment in core power fraction is comparatively low. At higher frequency, light is tightly confined in the core which results in increased ratio of confined area to the total area of the fiber. This phenomenon has been observed in Figure 5.20. By expanding the Core diameter in Figure 5.21, the absolute volume of air contrasted with the solid material in the core is reduced, which decreases the power fraction. At fixed diameter and frequency, the power fraction increases with core porosity which increases the amount of air inside the core. Thus higher amount of mode power flows through the core air slots. The core power fraction of our proposed photonic crystal fiber is 50% for 280μm core diameter and 90% core porosity.

5.5 Confinement Loss

PCFs are a new class of optical fibers, which has concerned fabulous attention in the last few years. PCFs are normally formed with silica having air holes positioned in the cladding region. PCFs have novel properties because the effective refractive index has burly wavelength dependence and huge design flexibility. PCFs main applications range from telecommunication field to metrology, spectroscopy, microscopy, medical diagnostics equipment, biology and sensing. There are several parameters to manipulate pitch, air hole shape and diameter, refractive index of the glass, and type of lattice. PCFs structures can have hexagonal lattice or octagonal lattice or square lattice. By changing the lattices and lattice parameters like pitch, air hole diameter and changing rings in the cladding region, the properties of PCFs can also be changed. Many experiments and investigations have been carried out using different analysis techniques and tools to understand the propagation properties of various PCFs. PCFs also known as micro-structured or holey fibers are made of the refractive index periodicity, with the arrangement of air holes around the core. Many rings around the core help to ensnare light well within the core minimizing the confinement loss. Based on structure, PCFs can be either solid core high-index guiding fibers or hollow core low index guiding fibers. The index guiding PCFs guide light in a solid core by modified total internal reflection (M-TIR) like to the conventional optical fibers. Hollow core PCFs guide light by the photonic band gap (PBG) effect. Light is confined in the low-index core, as the distribution of energy levels in the structure makes the propagation in the cladding region impossible. In both cases, to attain the lowest amount loss, air holes should be continual to infinity which is unfeasible. So modes leak in cladding and confinement loss is

created. The confinement loss can be reduced by proper design of structure parameters in PCFs, and consequently, mode leakage to cladding is avoided. Already, many reports have been published about PCFs with low confinement loss. At 0.8 µm center wavelength the confinement loss is found 10^{-8}dB/m, 10^{-6}dB/m and 10^{-4} dB/m for 2 µm, 1.8 µm and 1.6 µm lattice pitches. Again at 1.55 µm center wavelength for three rings hexagonal PCFs the confinement loss is 10^{-3} dB/km but Ademgil and Huxha obtained this loss which was varied from 10^{-1} to 10^{-5}dB/m [10]. also at 1.3 µm centers wavelength this confinement loss was found 10^{-8} dB/km for circular ring PCFs. Another important parameter to be considered for PCF design is confinement loss. It depends upon the core porosity and the number of air holes used in cladding. It can be calculated by taking the imaginary part of the complex refractive index. The confinement loss can be calculated by equation 5.4, [33].

$$\alpha_{CL} = 8.686 \times \frac{2\pi f}{c} \mathrm{Im}(\eta_{eff}) \qquad 5.4$$

Where, f is the frequency of the guiding light, c is speed of light in vacuum and Im(neff) symbolizes the imaginary part of the refractive index. The confinement loss as a function of frequency where it is observed that as the frequency increases, the confinement loss scaled down.

5.5.1 Proposed Octa square cladding with slotted core design.

It can be seen that from Figure 5.22 and Figure 5.23, confinement loss scales down with the increase of frequency. This happens because of strict confinement of light waves in core region at higher frequency. That is, less area from cladding gets affected. As a result the confinement loss decreases. By increasing the air hole in cladding region, confinement loss can be reduced further. Since increase in number of air holes results in less interaction of material with light and tight confinement. Apart from this it is also observed that confinement loss decreases with increase of core porosity and core diameter. Larger core diameter bears the chances of the confinement not being restricted to the center only. So, we have chosen some optimum points for operation such that we get minimized confinement loss. We have chosen D_{core} is 290 µm core diameters; f is 1.6 THz and 80% porosity to be optimum.

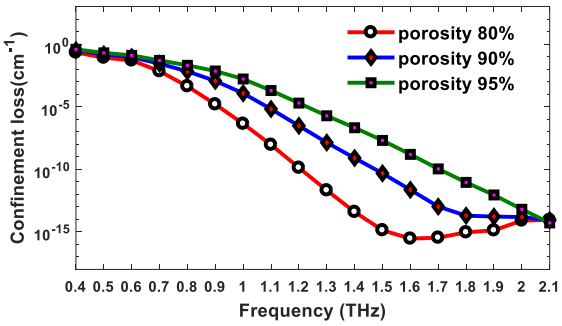

Figure 5.23: Confinement loss vs frequency at different core diameters for Octa square cladding with slotted core design

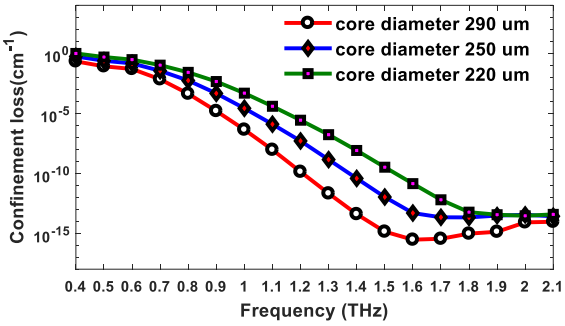

Figure 5.22: Confinement loss vs frequency at different core porosities for Octa square cladding with slotted core design.

The value of confinement loss we obtained from our proposed photonic crystal fiber is 10^{-15} cm^{-1} at 80% porosities of 290 um and 1.6 THz, core diameter and frequency respectively, which is better than earlier proposed [11, 12] optical waveguide.

5.5.2 Proposed hexagon cladding with slotted core design

One can deduce from figure 5.24 that confinement loss decreases rapidly with increasing frequency. This

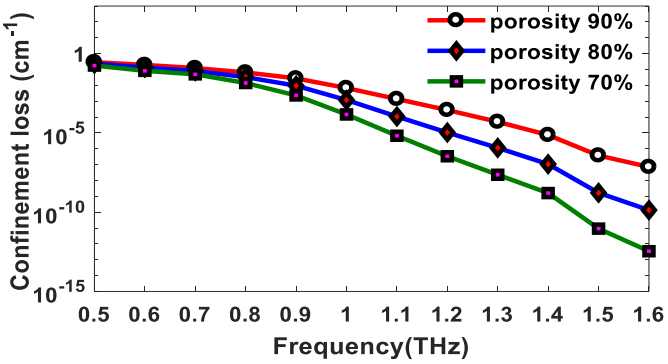

Figure 5.24. Confinement loss vs frequency at different porosities and core diameter = 270µm for hexagon cladding with slotted core design

Phenomenon is obvious since at higher frequencies mode power tightly confines in the slotted core region, and this results in a low confinement loss. One can also observe from the figure that the reduction of core porosity gives the same results. The reason for this phenomenon can be understood easily. When core porosity has been minimized, less air volume is faced by the guiding mode. Index contrast increases due to this, which is the reason for the significant reduction of confinement loss. For this PC-PCF the confinement loss is about $1.05x10^{-13}$ cm^{-1},

which is much lower than the previously reported designs [13, 14, 69, 70, 74]. This loss can be further decreased by inserting extra rings in the outer cladding.

5.5.3 Confinement loss of Octa circular cladding with slotted core design.

Figure 5.25 and Figure 5.26 both shows that confinement loss has an inverse relationship with the core diameter as well as frequency. Confinement loss decreases with the increment of both core diameter and frequency. The reason is at higher frequencies, light is strongly confined inside the slotted core region. As core diameter increases, the index contrast between core and cladding increase and light is tightly restrained hence it leads to scale down the confinement loss. Similarly, decreasing the core porosity causes light to confine well into the core region and so

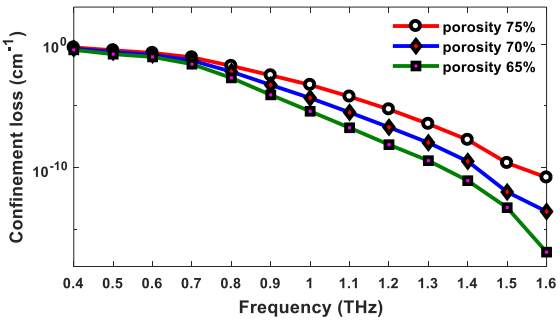

Figure 5.26: Confinement loss versus frequency at different porosities for Octa circular cladding with slotted core design.

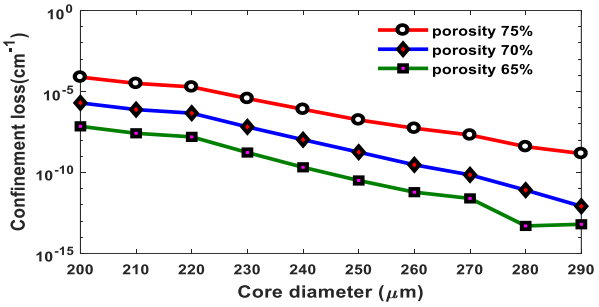

Figure 5.25: Confinement loss versus core diameter at different porosities for Octa circular cladding with slotted core design.

Confinement loss decreases. From the three porosity levels we obtained lowest confinement loss at 65% porosity which is 10^{-18}cm^{-1} at $D_{core} = 290\mu m$ and $f = 1.6THz$

5.5.4 Confinement loss of hexagon cladding with circular core design.

A standard PC-PCF must have narrow array of confinement loss. From Figure 5.27 it can be stated that Confinement loss decreases as the operating frequency increases. It can be justified by the fact that at higher frequency, light bounds strongly in the core region and less light is captured by the cladding air holes. Hence the confinement loss decreases at higher operating frequency. The optimum value of confinement loss we obtained from our proposed photonic crystal fiber is 10^{-14} cm^{-1} at 50% porosities of 280 µm core diameter and 1.5 THz frequency.

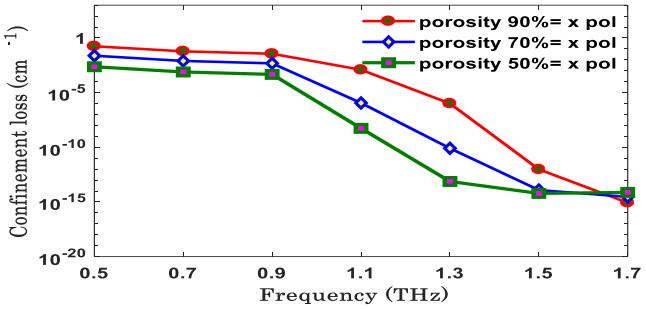

Figure 5.27: Confinement loss vs frequency at different core porosities for hexagon cladding with circular core design

5.6 Dispersion

In optics, dispersion is the phenomenon in which the phase velocity of a wave depends on its frequency. Media having this common property may be termed dispersive media. Sometimes the term chromatic dispersion is used for specificity. Although the term is used in the field of optics to describe light and other electromagnetic waves, dispersion in the same sense can apply to any sort of wave motion such as acoustic dispersion in the case of sound and seismic waves, in gravity waves (ocean waves), and for telecommunication signals propagating along transmission lines (such as coaxial cable) or optical fiber. In optics, one important and familiar consequence of dispersion is the change in the angle of refraction of different colors of light, as seen in the spectrum produced by a dispersive prism and in chromatic aberration of lenses. Design of compound achromatic lenses, in which chromatic aberration is largely cancelled, uses a quantification of a glass's dispersion given by its Abbe number V, where lower Abbe numbers correspond to greater dispersion over the visible spectrum. In some applications such as telecommunications, the absolute phase of a wave is often not important but only the propagation of wave packets or "pulses"; in that case one is interested only in variations of group velocity with frequency, so-called group-velocity dispersion (GVD).

5.6.1 Material and waveguide dispersion

Most often, chromatic dispersion refers to bulk material dispersion, that is, the change in refractive index with optical frequency. However, in a waveguide there is also the phenomenon of waveguide dispersion, in which case a wave's phase velocity in a structure depends on its frequency simply due to the structure's geometry. More generally, "waveguide" dispersion can occur for waves propagating through any inhomogeneous structure (e.g., a photonic crystal),

whether or not the waves are confined to some region. In a waveguide, both types of dispersion will generally be present, although they are not strictly additive. For example, in fiber optics the material and waveguide dispersion can effectively cancel each other out to produce a Zero-

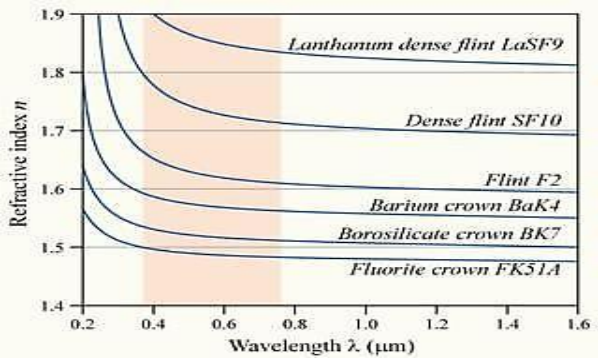

Figure 5.28 Material dispersion in optics

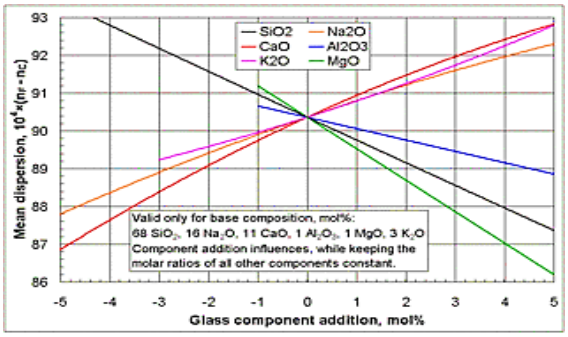

Figure 5.29 Mean dispersion in terms of mole

dispersion wavelength, important for fast Fiber-optic communication. The variation of refractive index vs. vacuum wavelength for various glasses. The wavelengths of visible light are shaded in red. Influences of selected glass component additions on the mean dispersion of a specific base glass (n_f valid for λ = 486 nm (blue), n_c valid for λ = 656 nm (red).Material dispersion can be a desirable or undesirable effect in optical applications. The dispersion of light by glass prisms is used to construct spectrometers and spectra radiometers. Holographic gratings are also used, as they allow more accurate discrimination of wavelengths. However, in lenses, dispersion causes chromatic aberration, an undesired effect that may degrade images in microscopes, telescopes and photographic objectives. In general, the refractive index is some function of the frequency f of the light, thus , n = n(f), or Alternatively, with respect to the wave's wavelength n = n(λ). The wavelength dependence of a material's refractive index is usually quantified by its Abbe number or its coefficients in an empirical formula such as the Cauchy or Sellmeier equations. Because of the Kramers–Kronig relations, the wavelength dependence of the real part of the refractive index is related to the material absorption, described by the imaginary part of the refractive index (also called the extinction coefficient). In particular, for non- magnetic materials ($\mu = \mu_0$), the susceptibility χ that appears in the Kramers–Kronig relations is the electric susceptibility $\chi_e = n^2 - 1$. The most commonly seen consequence of dispersion in optics is the separation of white light into a color spectrum by a prism. From Snell's law it can be seen that the angle of refraction of light in a prism depends on the refractive index of the prism material. Since that refractive index

varies with wavelength, it follows that the angle known as angular dispersion. In this case, the medium is said to have normal dispersion. Whereas, if the index increases with increasing wavelength (which is typically the case for X-rays, the medium is said to have anomalous dispersion. At the interface of such a material with air or vacuum (index of ~1), Snell's law predicts that light incident at an angle θ to the normal will be refracted at an angle arc sin(sin θ/n). Thus, blue light, with a higher refractive index, will be bent more strongly than red light, resulting in the well-known rainbow pattern.

5.7 Dispersion in waveguides

Waveguides are highly dispersive due to their geometry (rather than just to their material composition). Optical fibers are a sort of waveguide for optical frequencies (light) widely used in modern telecommunications systems. The rate at which data can be transported on a single fiber is limited by pulse broadening due to chromatic dispersion among other phenomena. In general, for a waveguide mode with an angular frequency ω(β) at a propagation constant β (so that the electromagnetic fields in the propagation direction z oscillate proportional to $e^{i(\beta z-\omega t)}$), the group-velocity dispersion parameter D is defined by the following equation 5.5, [34].

$$\beta_2 = \frac{2}{c}\frac{d\eta_{eff}}{d\omega} + \frac{\omega}{c}\frac{d^2\eta_{eff}}{d^2\omega} \quad \text{ps/THz/cm} \qquad 5.5$$

Where ω is the angular frequency and $\omega = 2\pi f$, f is the operating frequency, η_{eff} is the effective refractive index, and c is the speed of light.

5.7.1 Dispersion of Octa square cladding with slotted core design.

Figure 14 displays dispersion properties as a function of frequency. Dispersion properties flatten gradually with the increase of porosity and frequency. This occurs because at higher porosity air holes are compactly placed with each other and are steering to assuage the variation of index with frequency resulting in a flattened dispersion. The increased flatten dispersion properties we obtained from our proposed PCF is $0.3 \pm 0.1\ \text{ps/THz/cm}$ at a wide frequency range 0.7-2.1 THz, which is better than previously reported [12, 13, 14, 15] optical waveguides.

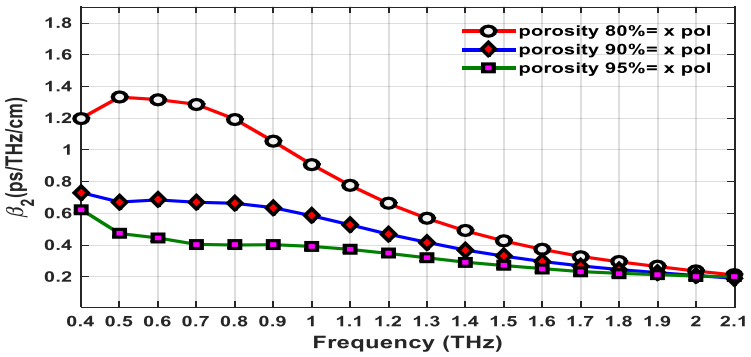

Figure 5.30: Dispersion vs frequency at different core porosities for Octa square cladding with slotted core design

5.7.2 Dispersion of hexagon cladding with slotted core design

It can be seen from Figure 5.31 that dispersion properties flatten slowly with increasing the core porosity and frequency, respectively. This is because, at higher core porosity, air slots in the core

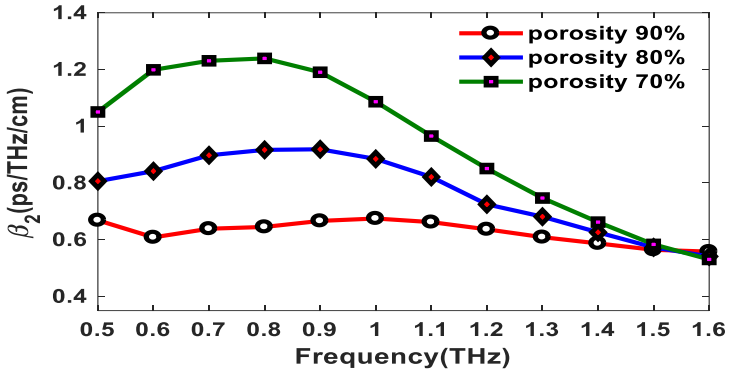

Figure 5.31. Dispersion vs frequency for hexagon cladding with slotted core design.

are placed compactly with each other and assist in reducing the variation of the index and facilitating dispersion to flatten more. Flat dispersion is essential in THz wave guiding because it allows transmitting several optical signals at the same time with nearly equal pulse spreading. From our proposed design, we obtained dispersion 0.65±0.05 ps/THz/cm between frequency ranges 0.6-1.6 THz at porosity 90%. This variation is much lower than most of the previously reported designs [12, 14, 62, 70, 74].

5.7.3 Dispersion of Octa circular cladding with slotted core design

By observing Figure 5.32 we can say that at low porosities and low frequencies, up to 0.6 THz, the dispersion variation for x-polarization mode is quite high. But from 0.6THz to 1.6THZ the

proposed fiber displays Flattened dispersion. The reason behind this is at higher porosity the core air holes are placed air-tightly with each other which alleviate the variation of index with frequency thus the dispersion becomes more flattened. The obtained flattened dispersion from our proposed PCF is 0.6 ± 0.16 ps/THz/cm at a wide frequency range 0.4-1.6 THz.

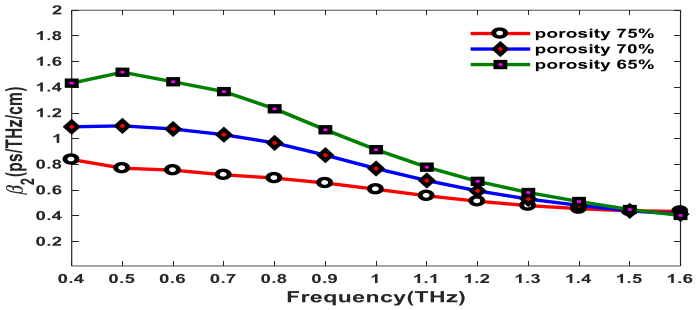

Figure 5.32: Dispersion vs frequency at different porosities for Octa circular cladding with slotted core design.

5.7.4 Dispersion of hexagon cladding with circular core design

Figure 5.33 displays the dispersion properties as a function of frequency. The flattened

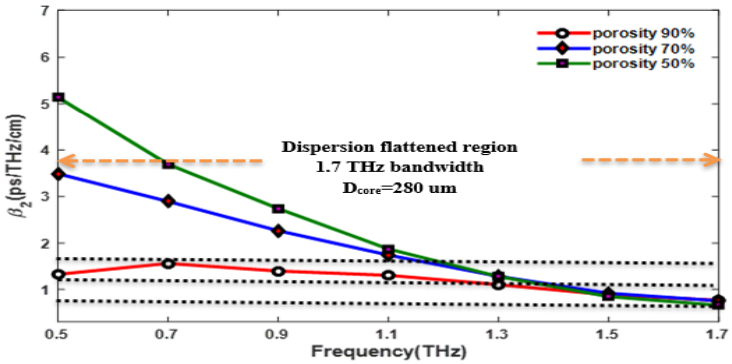

Figure 5.33: Dispersion vs frequency at different porosities for hexagon cladding with circular core design

dispersion we obtained from our proposed PCF is 1.03±0.04 ps/THz/cm at a large frequency range from 0.9 THz to 1.5 THz at 90% porosity. At higher porosity, air holes are more tightly confined resulting in less variation in refractive index.

5.8 Effective Area

Effective area depends on the amount of light confined in the core. Effective area has been characterized by following equation 5.6, [35]. Where $I(r)$ is the transverse electric intensity distribution and it characterized by the $I(r) = |E_t|^2$.

$$A_{eff} = \frac{\left[\int I(r) r dr\right]^2}{\left[\int I^2(r) dr\right]^2} \qquad 5.6$$

5.8.1 Effective Area of Octa square cladding with slotted core design

Figure 5.34 reflects the alteration of effective area as a function of frequency at different porosities. Effective area decreases with the increase of frequency and the decrease of core porosity. At higher porosity, the fiber is more porous and prone to interacting with light. Light can be confined more intensely and tightly at the core if the fiber is made more porous. Thus the light affected area increases if we increase the porosity of our designed fiber. As frequency progresses,

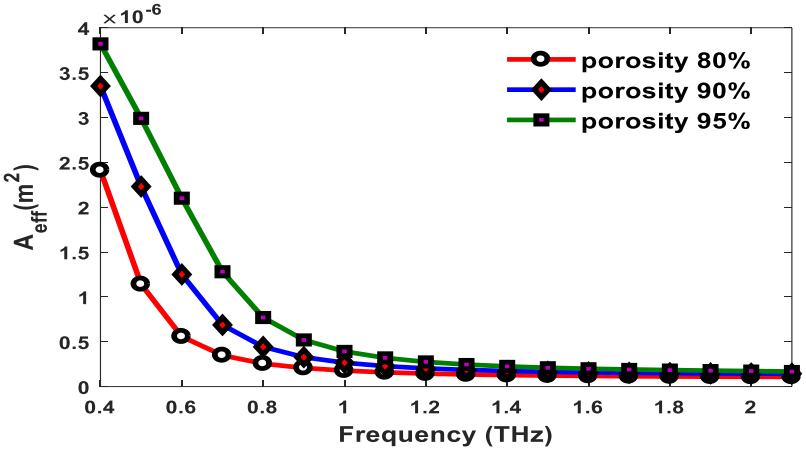

Figure 5.34: Effective area vs frequency at different core porosities for Octa square cladding with slotted core design.

the effective area decreases and at a point, the decrement saturates and the curve becomes flattened. Our proposed fiber has an effective area of about 4×10^{-6} m^2 at the optimum characterizing values of frequency and porosity.

5.8.2 Effective Area Octa circular cladding with slotted core design

The effective mode area of the proposed PCF is shown in Figure 5.35. It shows that effective mode area decreases with increase in frequency. At higher frequencies, the mode field is emphatically confined inside the core air slot [31], diminishing the effective area secured by the mode. Furthermore increasing the porosity causes the effective area to increase which is evident in Figure 12. Since the index contrast between the cladding and the core is reduced with

increasing porosity, the mode field starts to expand from the core which increases the effective area. The effective area of proposed PCF is about 2.8×10^{-6} m^2.

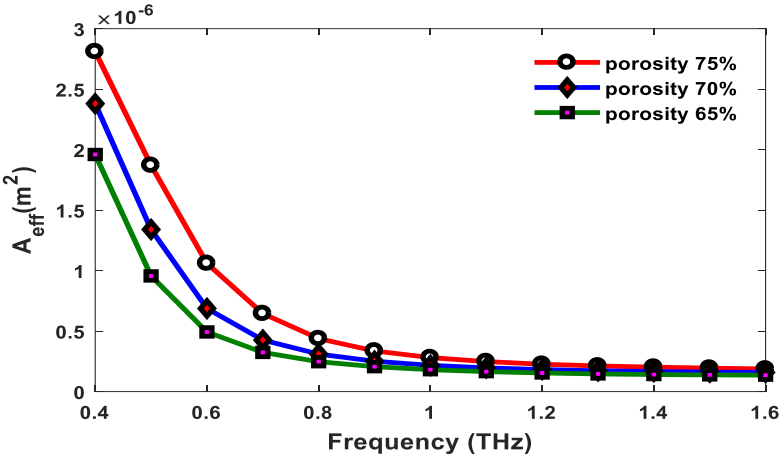

Figure 5.35: Effective area versus frequency at different porosities for Octa circular cladding with slotted core design

5.8.3 Effective Area of hexagon cladding with circular core design.

Figure 5.36 shows the alteration of effective area as a function of frequency. Effective area has decreased with increase of frequency as well as decrease of core porosity. Because at higher porosity index contrast between cladding and core increases. Eventually mode starts to expand from the core and effective area increases. The effective area of the proposed fiber is about 1.4×10^{-6} m^2 at 90% porosity and operating frequency at 0.5THz.

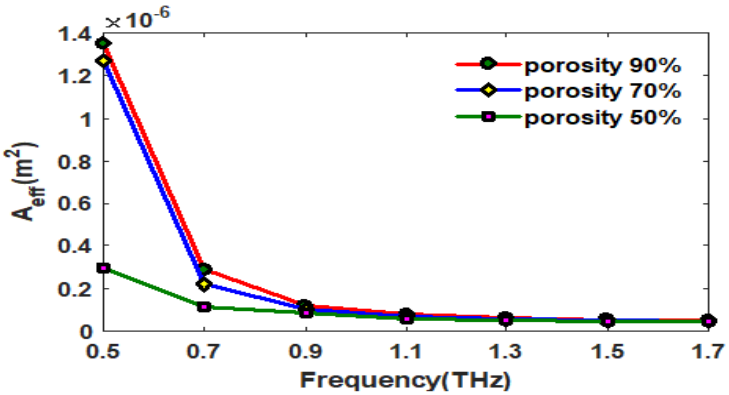

Figure 5.36: Effective area vs frequency at different core porosities for hexagon cladding with circular core design

5.9 Numerical aperture

Numerical aperture is another important parameter for photonic crystal fiber. In fiber optics, it is described as the range of angles within which light incident on the fiber will be transmitted along it. This is demonstrated by following equation 5.7, [37].

$$NA = \frac{1}{\sqrt{1+\frac{\pi A_{eff} f^2}{c^2}}} \qquad 5.7$$

Here A_{eff} is effective area of the core and f is the normalized frequency and c is the speed of light

5.9.1 Numerical aperture of Octa square cladding with slotted core design

Figure 5.37 displays the change of numerical aperture as a function of frequency and also with porosity. The characteristic curve is at first increasing for a bit and then decreasing with the increase of frequency. With increasing frequency and core porosity, Numerical Aperture will first try to increase from its initial position in the curve and then decrease for the rest of the curve.

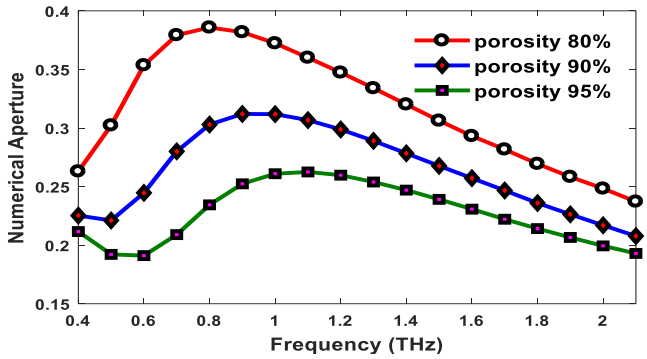

Figure 5.37: Numerical Aperture vs frequency at different core porosities for Octa square cladding with slotted core design

This effect can be examined from the formula of numerical aperture. In the formula, we have effective area in the denominator. From previous section (Figure 5.37) it is evident that effective area gets scaled down and eventually become flattened more and more at decreasing porosity. Numerical Aperture has an inverse correspondence to effective area $A_{eff.}$ This characterization amounts to porosity being an inverse factor for numerical aperture that is with increasing porosity, Numerical Aperture will decrease.

5.9.2 Numerical aperture of Octa circular cladding with slotted core design

From Figure 5.38, we can say that despite some early increase, the numerical aperture decreases almost linearly with frequency, and it is higher at lower core porosity.

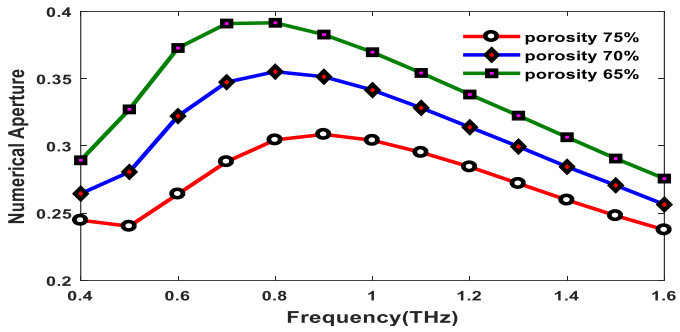

Figure 5.38: Numerical aperture versus frequency at different porosities

5.9.3 Numerical aperture of hexagon cladding with circular core design.

Figure 5.39 demonstrates the change of numerical aperture as a function of frequency and also with porosity. At higher porosity, numerical aperture decreases with frequency.

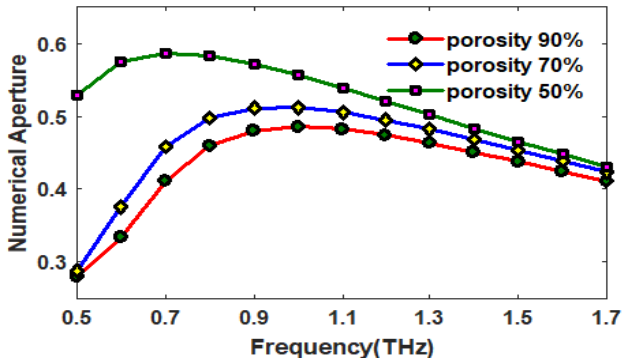

Figure 5.39: Numerical Aperture vs frequency at different core porosities for hexagon cladding with circular core design

5.10 Birefringence

Typically, birefringence induced in a porous core PCF occurs by breaking the symmetric characteristics of the core or cladding and separating the light into two polarized components (x-polarization and y-polarization) [45]. Birefringence is known to be the refractive index difference between x polarization mode and y polarization mode. So it basically refers to the physical origin of the separation, which is the existence of a variation in refractive index that is

sensitive to direction in a geometrically ordered material. This is expressed by following formula [34].

$$B = \left| n_x - n_y \right| \qquad 5.8$$

Where B denotes birefringence of following crystal fiber, n_x and n_y represents the refractive index of x polarization mode and y polarization mode respectively.

5.10.1 Birefringence of Octa square cladding with slotted core design

Typically, birefringence induced in a porous core PCF occurs by breaking the symmetric characteristics of the core or cladding and separating the light into two polarized components (x-polarization and y-polarization) [45]. Birefringence is known to be the refractive index difference between x polarization mode and y polarization mode. So it basically refers to the physical origin of the separation, which is the existence of a variation in refractive index that is sensitive to direction in a geometrically ordered material.

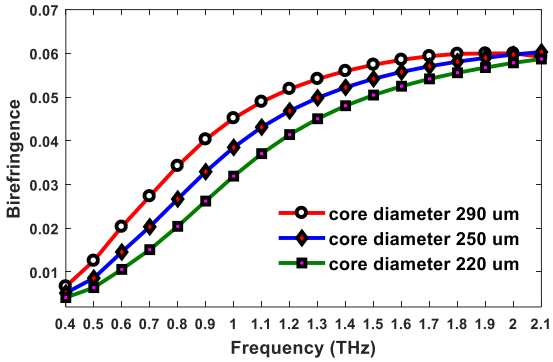

Figure 5.41: Birefringence vs frequency at different core diameters for Octa square design

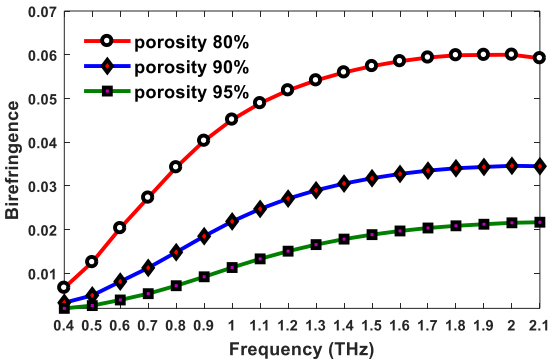

Figure 5.40: Birefringence vs frequency at different core porosities for Octa square design

Figure 5.40 and Figure 5.41 represent the variation of birefringence as a function of frequency for different core porosities and core diameters consequently. It is notified from above figure that the value of refractive index is proportional to core diameter and inversely proportional to core porosity. This eventuates increasing the core diameter gives the light an increased opportunity to pass through. Thus when core diameter increases, refractive index increases. This results in an increment of difference between the refractive indices hence birefringence increases. Again, increasing the number of air holes or porosity, we can restrict the birefringence to a lower value.

This can be validated from our result as we can detect that the birefringence of our proposed photonic crystal fiber is 0.06 which is comparable with the other proposed fiber in the past.

5.10.2 Birefringence of hexagon cladding with slotted core design

Figure 5.42 depicts that for a particular frequency, higher core porosity provides lower birefringence value. The reason is that at a higher porosity, the mode field is delocalized from the core and spread into the cladding, which results in the reduction of the index contrast between two orthogonal polarization modes. As a consequence, less power is controlled by the slots, and birefringence is reduced. It is also observed in figure 5.42 that the bandwidth of birefringence. Increases with the decrement of core porosity. For example, for porosity 70%, birefringence is higher than 0.06 within 0.8–1.6 THz frequency band, whereas for porosity 80%, the birefringence stays above 0.06 within a narrower band of 0.91–1.6 THz and the band is narrowed

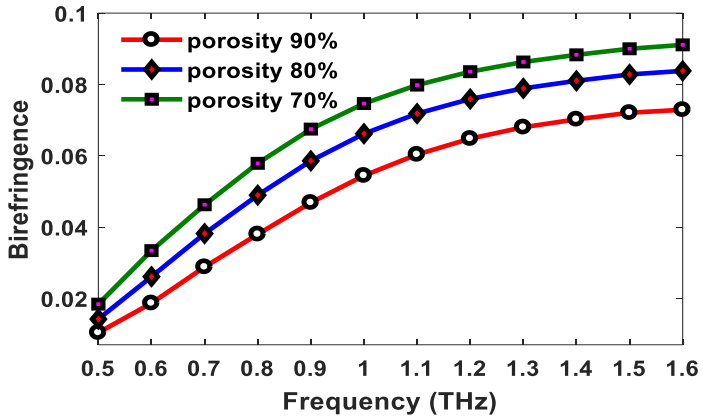

Figure 5.42. Birefringence vs frequency at different porosities for hexagon cladding with slotted core design

Down to 1.1–1.6 THz for porosity 90%. The highest birefringence of ~0.0911 can be obtained from this design for core diameter 270 μm and porosity 70% at frequency 1.6 THz which is to the best of our knowledge, is the highest birefringence value reported to date [51, 58-61]. Besides this, one can see from figure 5 that birefringence stays above 0.08 for frequency range 1.1–1.6 THz, which is wider than the previously reported works [15, 52, 75-86].

5.10.3 Birefringence of Octa circular cladding with slotted core design

From the illustrated Figure 5.43 we can see that, the birefringence increases gradually with the frequency up to 1.3THz then it becomes almost flatten from 1.3THz to 1.6THz. The increment

occurs because of the improvement of index contrast between the core and cladding at higher frequencies. It is additionally seen that the birefringence decreases with the increment of porosity. This is in view of the fact that at higher porosities some of mode power going out from core to cladding, lessening the index contrast between two polarization modes. Eventually birefringence decreases.

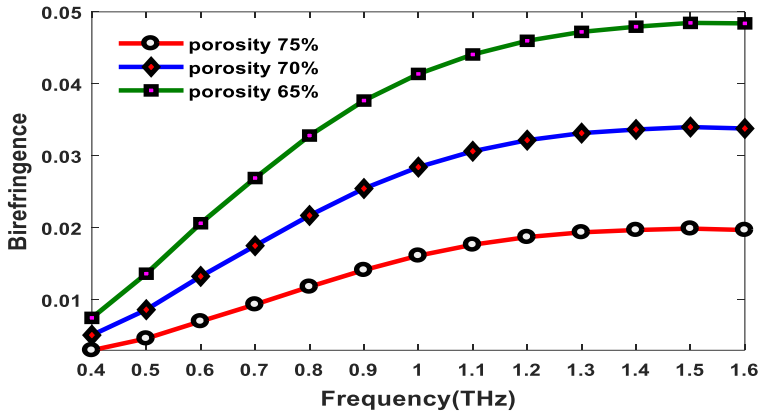

Figure 5.43: Birefringence versus frequency at various porosities for Octa circular cladding with slotted core design

5.11 Conclusion

We investigated octagonal and hexagonal shaped porous core PCF for Terahertz applications and analyzed numerically with respect to frequency, core diameter and core porosity. Octagonal and hexagonal shaped cladding region is used to ensure low effective material loss, high core power fraction along with flattened dispersion properties and with high birefringence. The high birefringence and the formidable guiding characteristics make the suggested fiber a superlative candidate for fabrication of optical devices, medical diagnostics equipment, low-loss polarization applications and effective THz-wave transmission. We hope in future more accurate application of optical fiber designed PCF will be used for ensuring low confinement loss while having higher frequency range.

Chapter 6

Conclusion

6.1. Conclusion

In this book various types of photonic crystal fiber is demonstrated and its guiding properties are characterized for different values of core porosities and operating frequencies. This all proposed structure offers relatively low effective material loss, very small confinement loss and a flattened dispersion profile achieved for the optimal design parameters which is suitable for efficient THz wave guidance. All structure can be manufactured due to its realistic dimension that facilitates practical fabrication. A relatively simple hexagonal cladding with circular core photonic crystal fiber is demonstrated. The porous core made it possible to exhibit a low EML of 0.029 cm^{-1}, 50% core power fraction, confinement loss of 10^{-14} cm^{-1} at 90% porosity. In addition to this we obtained near flat dispersion of 1.03±0.04 ps/THz/cm for a wide range starting from 0.9 THz to 1.5 THz. Another hexagonal cladding with slotted core PCF is designed here, and its key feature is ultra-high birefringence (0.091) and very low EML (0.025 cm^{-1}). Moreover, an adequate amount of modal power is transmitted through the core that results in high core power fraction, and the compact arrangement of air holes in the cladding helps to maintain low confinement loss. The single-mode propagation of the proposed design has been justified for different core porosities and core diameters. A more effective octagonal shaped cladding with slotted core PCF is introduced next where high birefringence is obtained from our result which is 0.06 at 1.6 THz Frequency. The proposed PCF offers us a low EML of 0.06 cm^{-1}, a negligible confinement loss of 10^{-15} cm^{-1}, a flattened dispersion variation of 0.3±0.1 ps/THz/cm, along with a very high core power fraction of 70% for 290 µm core diameter with a core porosity of 80% and a large modal effective area of 4×10^{-6} m^2 over a wide range of frequencies. This PCF also offers an ultra-low EML of 0.007 at 0.5 THz. Another last one octagon circular cladding photonic crystal fiber (PC-PCF) structure with slotted rectangular air gap core has been proposed. From the simulation results, we have accomplished remarkable outcomes. We achieved effective material loss (EML) of 0.013 cm^{-1} and a high birefringence of 0.05 at 1.6THz. In addition to that, the proposed structure offers 60% high core power fraction, 10^{-18} cm^{-1} confinement loss at 65% porosity of 290

μm core diameter and 1.6 THz frequency. Furthermore the effective area is nearly 2.8×10^{-6} m^2, near zero flat dispersion of $0.6 \pm 0.16 ps / THz / cm$ is obtained. This all micro-structure PCFs can be a potential waveguide in Terahertz radiation propagation. Therefore, it is quite evident that, the proposed fibers can be a potential candidate for a long-distance terahertz wave transmission and other practical applications such as fiber-optic communication, fiber laser, non-linear devices etc. for its simple structure and significantly enhanced properties.

6.2. Possible fabrication methods

Fabrication is an important issue to consider for PCFs. Fortunately, fabrication precision and accuracy are progressing gradually day by day. PCFs are produced by a number of distinct methods which generally involve preparing a macroscopic meter-length preform with the desired transverse crystal lattice pattern and draw into microscopic scale fibers while preserving the intended cross-sectional design. Some examples of PCF fabrication methods are stack-and-draw, extrusion [77], sol-gel casting [78], injection molding [79] and drilling [80]. The most common method is stack-and- draw technique, devised by Knight et al. [80], which is relatively fast, clean, low-cost, and flexible. Here, we report fabrication of silica HIG PCF in UM using this method. A 5m high fiber drawing tower with furnace heating capability up to 2700 ºC is used. Stack-and-draw process is most important method. This method begins with fabricating capillaries of required sizes with specific inner wall over outer wall diameter ratio (ID/OD) based on PCF whole diameter, d, over lattice spacing, ä, ratio (d/ä) determined in design. Next, fabricated capillaries are arranged into triangular lattice using custom-made jigs. Subsequently, by using fiber drawing facilities, the assembled PCF preform is pulled into fiber by adjusting carefully the feeding rate, tractor speed and furnace temperature. Most recently, a research group of max Planck University has fabricated PCFs of different sizes and complicated structures by using the well-known stack and draw technique [81]. It is anticipated that existing fabrication technology will not encounter any difficulty while fabricating the proposed PCFs because the designs are comprised of porous-core and air hole cladding. The ability of fabricating PCF opens up new fiber design possibilities and practically harnessing various unique properties of PCF.

6.3. Scope for Future Works

There are some drawback of our proposed design is power fraction can be further increased and EML can be further decreased. Still the accumulated result is satisfactory and can be developed in further purpose. So the future goal should be developing a fabrication process for this accumulated design which is efficient and easy so that worldwide it can be adopted. Furthermore, simulations should be continued for new design so that low EML and high power fraction design can be adopted and fabricated practically. Also the High birefringence can be obtained by using dual unit based porous core and rotating core air holes at different angles. High birefringence with reasonable EML can also be achieved by using microstructure cladding air holes and elliptical core air holes.

References

1. J C Knight, T A Birks, P S J Russell, and D M Atkin, “All-silica single-mode optical fiber with photonic crystal cladding,” Optics Letters, Vol. 21, no. 19,pp. 1547–1549, September, 1996.
2. Huttunen, A., and Törmä, P.,“Effect of wavelength dependence of nonlinearity, gain, and dispersion in photonic crystal fiber amplifiers”. Optics Express, Vol.13, no.11, pp. 4286, December, 2015..
3. Z Tan, X Hao, Y Shao, Y Chen, X Li, and P Fan, Phase modulation and structural effects in a D-shaped all-solid photonic crystal fiber surface Plasmon resonance sensor. Optics Express, Vol.22, no.12, pp. 15049, March, 2014.
4. T V Ramanaa, A Pandianb, C Ellammalc, T Jarind, Ahmed Nabih Zaki Rashede, A Sampath Kumar, “Numerical analysis of circularly polarized modes in coreless photonic crystal fiber”. Elsevier B.V. (February, 2019).
5. Y. Zhu, Z. He, and H. Du, “Detection of external refractive index change with high sensitivity using long-period gratings in photonic crystal fiber,” Sensors and Actuators B, vol. 131, no. 1, pp. 265–269, October, 2008.
6. Shiju Chacko, Jeena Maria Cherian, Sunilkumar K, “Low Confinement Loss Photonic Crystal Fiber (PCF) With Flat Dispersion over C-Band”, International Journal of Computer Applications, Vol. 85, no.15, December, 2013.
7. Mortensen, N. A., Folken, J. R., Skovgaard, P. M. W., and Broeng, J. (2002). “Numerical aperture of single-mode photonic crystal fibers”, IEEE Photonics Technology Letters, Vol.14, no.8, pp. 1094–1096, March, 2017..
8. Yang, T., Wang, E., Jiang, H., Hu, Z., and Xie, K. (2015). High birefringence photonic crystal fiber with high nonlinearity and low confinement loss. Optics Express, Vol. 23, no.7, pp.8329, march 2016..
9. Tan, X., Geng, Y., Li, E., Wang, W., Wang, P., and Yao, J. (2008). “Characterization of bent large-mode-area photonic crystal fiber”, Journal of Optics A: Pure and Applied Optics, Vol.10, no.8, pp. 085303, October, 2015.
10. Vu, N. H., Hwang, I.-K., and Lee, Y.-H. (2008). Bending loss analyses of photonic crystal fibers based on the finite-difference time-domain method. Optics Letters, Vol. 33, no.2, pp. 119,August, 2018,

11. Ali, S., Sarkar, T., Day, A., Hasan, M. R., Mou, J. R., Rana, S., Ahmed, N. (2016). "Ultra-low loss THz waveguide with flat EML and near zero flat dispersion properties. 2016 9th International Conference on Electrical and Computer Engineering (ICECE).
12. P S Maji and Roy Chaudhuri, "Super continuum generation in ultra-flat near zero dispersion PCF with selective liquid infiltration", Optic - International Journal for Light and Electron Optics, Vol. 125, no.20, pp.5986–5992,july, 2017.
13. Lin, P., Li, Y., Cheng, T., Suzuki, T. and Ohishi, Y. Coexistence of Photonic Bandgap Guidance and Total Internal Reflection in Photonic Crystal Fiber Based on a High-Index Array with Internal Air Holes", IEEE Journal of Selected Topics in Quantum Electronics, Vol. 22, no.2, pp. 265–270, March, 2016.
14. H.Han, H.Park, M.Cho and J.Kim, "Terahertz pulse propagation in a plastic photonic crystal fiber," Appl.Phys. Lett. Vol. 80, pp.2634–2636, November 2002.
15. S. Asaduzzaman and K. Ahmed, "Proposal of a gas sensor with high sensitivity, birefringence and nonlinearity for air pollution monitoring," Sensing and Bio-Sensing Research, Vol.10, pp. 20–26, December, 2016.
16. Lu, Y., Hao, C.-J., Wu, B.-Q., Musideke, M., Duan, L.-C., Wen, W.-Q. and Yao, J.-Q,"Surface Plasmon Resonance Sensor Based on Polymer Photonic Crystal Fibers with Metal Nanolayers. Sensors", Vol. 13, no.1, pp.956–965, November, 2013.
17. Muduli, N., Achary, J. S. N., and Padhy, H. ku, "Grade-2 Teflon (AF1601) PCF for optical communication using 2D FDTD technique: a simplest design". Journal of Modern Optics, Vol.63, no.7, pp. 685–691, June, 2017..
18. Shuvo Sen, Sawrab Chowdhury, Kawsar Ahmed, Sayed Asaduzzaman,"Design of a Porous Cored Hexagonal Photonic Crystal Fiber Based Optical Sensor With High Relative Sensitivity for Lower Operating Wavelength," Photonic Sensor , Vol. 7, No. 1, pp. 55–65 , March 2017.
19. Z. L. Liu, J. An, J. W. Xing, and H. L. Du, "Polarization rotator based on liquid crystal infiltrated tellurite photonic crystal fiber," Optic International Journal for Light and Electron Optics, Vol. 127, no.10, pp. 4391–4395, April, 2016.
20. G. Woyessa, A. Fasano, A. Stefani, C. Markos, K. Nielsen, H. K. Rasmussen, and O. Bang, "Single mode step-index polymer optical fiber for humidity insensitive high

temperature fiber Bragg grating sensors," Opt. Express, Vol. 24, pp.1253–1260, march, 2016.

21. A. Hassani, A. Dupuis, and M. Skorobogatiy, "Low loss porous terahertz fibers containing multiple subwavelength holes," Appl. Phys. Lett. Vol. 92, pp. 071101, January, 2008.
22. A. Dupuis, K. Stoeffler, B. Ung, C. Dubois, and M. Skorobogatiy, "Transmission measurements of hollow-core THz Bragg fibers," J. Opt. Soc. Am. B, Vol. 28, pp. 896–907 ,October, 2011.
23. M. Uthman, B.M.A. Rahman, N. Kejalakshmi, A. Agrawal, and K.T.V. Grattan, "Design and characterization of low-loss porous-core photonic crystal fiber," IEEE Photon. J. Vol.4, pp. 2315 –2325, December, 2012.
24. K. Tsuruda, M. Fujita, and T. Nagatsuma, "Extremely low-loss terahertz waveguide based on silicon photonic-crystal slab," Opt. Express, Vol. 23, pp. 31977–31990, September, 2015.
25. Md. Saiful Islama, Jakeya Sultanaa, Mohammad Faisal, Mohammad Rakibul Islam, Alex Dinovitser, Brian W-H. Ng, Derek Abbott, "A modified hexagonal photonic crystal fiber for terahertz applications," Elsevier Optical Fiber Technology, vol. 79, pp. 336–339, May 2018.
26. Fahad Ahmed, Subrata Roy, Kawsar Ahmed, Bikash Kumar Paul,Ali Newaz Bahar, "A novel star shape photonic crystal fiber for low loss terahertz pulse propagation", Nano Communication Networks, Vol. 19,pp.26–32 , October 2019.
27. M. A. Habiba, and M. S. Anower , "Square Porous Core Microstructure Fiber for Low Loss Terahertz Applications", Optics and Spectroscopy, Vol. 126, No. 5, pp. 607–613, July, 2019.
28. Reyes-Vera, E., Usuga-Restrepo, J., Jimenez-Durango, C., Montoya-Cardona, J. and Gomez-Cardona, N. "Design of Low-loss and Highly Birefringent Porous-Core Photonic Crystal Fiber and Its Application to Terahertz Polarization Beam Splitter," IEEE Photonics Journal, vol. 10, no. 4, pp. 1–13, August 2018.
29. Md. Sohidul Islam, Jamilur Rahman and Mohammad Rakibul Islam, "Topas Based Low Loss and Dispersion Flatten Decagonal Porous Core Photonic Crystal Fiber for Terahertz Communication", International Journal of Microwave and Optical Technology, Vol. 14, No. 1, January 2019.

30. Dhanu Krishna, G., Mahadevan Pillai, V. P. and Gopchandran, K. G.,"Design of low dispersion and low loss photonic crystal fiber: Defected core circular-octagon hybrid lattices", Optical Fiber Technology, Vol. 51,pp 17–24, November, 2019.
31. Cunningham, P.D., Valdes, N.N., Vallejo, F.A., Hayden, L.M., Polishak, B., Zhou, X.H., Luo, J., Jen, A.K.Y., Williams, J.C., Twieg, R.J,"Broadband terahertz characterization of the refractive index and absorption of some important polymeric and organic electro-optic materials". J. Appl. Phys. Vol. 109, pp. 043505 April, 2011.
32. A. Dupuis, J.-F. Allard, D. Morris, K. Stoeffler, C. Dubois, and M.Skorobogatiy, "Fabrication and THz loss measurements of porous sub wavelength fibers using a directional coupler method," Opt. Express, Vol. 17, pp. 8012–8028, December, 2009..
33. A. Dupuis, A. Mazhorova, F. Desevedavy, M. Roze, and M. Skorobogatiy,"Spectral characterization of porous dielectric sub wavelength THz fibers fabricated using a microstructure molding technique," Opt. Express, Vol. 18, pp. 13813–13828, July, 2010.
34. C. S. Ponseca, R. Pobre, E. Estacio, N. Sarukura, A. Argyros, M. C. J. Large,and M. A. van Eijkelenborg, "Transmission of terahertz radiation using a microstructure polymer optical fiber," Opt. Lett, Vol.33, pp. 902–904, March, 2008.
35. S. Atakaramians, S. Afshar Vahid, M. Nagel, H. Ebendorff-Heidepriem,B. M. Fischer, D. Abbott, and T. M. Monro, "THz porous fibers:design, fabrication and experimental characterization," Opt. Express, Vol. 17, pp. 14053–14062 ,February, 2009.
36. Jakeya Sultana, Md. Saiful Islam, Mohammad Faisal, Mohammad Rakibul Islam, Brian W.-H. Ng, Heike Ebendorff-Heidepriem, Derek Abbott, "Highly Birefringent elliptical core photonic crystal fiber for terahertz application," Optics Communications, vol. 407, pp. 92–96, January 2018.
37. Hasanuzzaman, G. K. M., Sohel Rana, and Md Selim Habib. "A Novel Low Loss, Highly Birefringent Photonic Crystal Fiber in THz Regime.", IEEE Photonics Technology, Vol. 28, no. 8, pp. 899-902, April, 2016.
38. Ahmed, Kawsar, Sawrab Chowdhury, Bikash Kumar Paul, Md Shadidul Islam, Shuvo Sen, Md Ibadul Islam, and Sayed Asaduzzaman. "Ultrahigh Birefringence,

Ultralow Material Loss Porous Core Single-Mode Fiber for Terahertz Wave Guidance.", Applied optics, Vol. 56, no. 12,pp. 3477-3483, January, 2017.

39. Islam, Md Saiful, Jakeya Sultana, Alex Dinovitser, Brian W-H. Ng, and Derek Abbott. "A Novel Zeonex Based Oligoporous-Core Photonic Crystal Fiber for Polarization Preserving Terahertz Applications.", Optics Communications, Vol. 413, pp. 4145-4152, August, 2018.
40. Hasan, Md Rabiul, Md Shamim Anower, Md Ariful Islam, and S. M. A. Razzak. "Polarization-Maintaining Low-loss Porous-Core Spiral Photonic Crystal Fiber for Terahertz Wave Guidance.",, Applied optics, Vol. 55, no. 15, pp. 4145-4152, May, 2016.
41. Luo, Jianfeng, Fengjun Tian, Hongkun Qu, Li Li, Jianzhong Zhang, Xinhua Yang, and Libo Yuan. "Design and Numerical Analysis of a THz Square Porous-Core Photonic Crystal Fiber for Low Flattened Dispersion, Ultrahigh Birefringence.", applied optics, Vol. 56, no. 24, 6993-7001, April, 2017.
42. Wu, Zhiqing, Xiaoyan Zhou, Handing Xia, Zhaohua Shi, Jin Huang, Xiaodong Jiang, and Weidong Wu. "Low-loss Polarization-Maintaining THz Photonic Crystal Fiber with a Triple-Hole Core.", applied optics, Vol. 56, no. 8, pp. 2288-2293, May, 2017.
43. Habib, Md Ahasan, and Md Shamim Anower. "Design and Numerical Analysis of Highly Birefringent Single Mode Fiber in THz Regime.", Optical Fiber Technology, Vol. 47, pp.197-203, March, 2019.
44. Tianyu Yang , Can Ding , Member, IEEE, Richard W. Ziolkowski, Fellow, IEEE, Fellow, OSA, and Y. Jay Guo , Fellow, IEEE, “A Scalable THz Photonic Crystal Fiber With Partially-Slotted Core That Exhibits Improved Birefringence and Reduced Loss,” Journal of light wave technology , vol. 36, no. 16, pp. 3408 – 3417, June, 2018.
45. Y. F. He, P.I. Ku, J.R. Knab, J.Y. Chen, A.G. Markelz, "Protein Dynamical Transition Does Not Require Protein Structure," Physical Review Letters, vol. 101, p. 178103, October, 2008.
46. J. Q. Zhang, D. Grischkowsky, "Waveguide terahertz time-domain spectroscopy of nanometer water layers," Optics Letters, vol. 29, pp. 1617-1619, January, 2004.
47. L. Ho, M. Pepper, P. Taday, "Terahertz spectroscopy: Signatures and fingerprints," Nature Photonics, vol. 2, pp. 541, December, 2008.

48. C. J. Strachan, P.F. Taday, D.A. Newnham, K.C. Gordon, J.A. Zeitler, M. Pepper, T. Rades, "Using Terahertz Pulsed Spectroscopy to Quantify Pharmaceutical Polymorphism and Crystallinity," Journal of Pharmaceutical Science, vol. 94, pp. 837-846, June, 2005.

49. N. Laman, S. S. Harsha, D. Grischkowsky, and J. S. Melinger, "7 GHz resolution waveguide THz spectroscopy of explosives related solids showing new features," Opt. Express, Vol. 16, pp. 4094–4105, November, 2008.

50. Q. Chen, Z.P. Jiang, G.X. Xu, X.C. Zhang, "Near-field terahertz imaging with a dynamic aperture," Optics Letters, vol. 25, pp. 1122-1124, March, 2000.

51. M. Nagel, Bolivar, P. H., Brucherseifer, M., Kurz, H., Bosserhoff, A. and Büttner, R., "Integrated THz technology for label-free genetic diagnostics," Applied Physics Letters, vol. 80, pp. 154-156, January, 2002

52. . D. Pinto and S. S. A. Obayya, "Improved complex-envelope alternating direction-implicit finite-difference-time-domain method for photonic band gap cavities," J. Lightw. Technol., vol. 25, no. 1, pp. 440–447, January, 2007.

53. M. Skorobogatiy and A. Dupuis, "Ferroelectric all-polymer hollow Bragg fibers for terahertz guidance," Appl. Phys. Vol. 90, no. 11, pp. 113514 , October, 2007.

54. Md.Saiful Islam, Sohel Rana, Mohammad Rakibul Islam, Mohammad Faisal, Hasan Rahman, Jakeya Sultana, "Porous core photonic crystal fiber for ultra-low material loss in THz regime,'' IET Communications, Vol.10, no.16, pp. 2179 – 2183, October 2016.

55. Sohel Rana, Golam Kibria, Md. Hasanuzzaman, Samiul Habib, Shubi F. Kaijage, Raonaqul Islam "Proposal for a low loss porous core octagonal photonic crystal fiber for T-ray wave guiding," Optical Engineering, Vol. 53, no. 11 , pp. 115107, November 2014.

56. B. Bowden, J. A. Harrington, and O. Mitrofanov, "Silver/polystyrene-coated hollow glass waveguides for the transmission of terahertz radiation," Optic Letters, vol. 32, pp. 2945-2947, February, 2007.

57. A. Dupuis, K. Stoeffler, B. Ung, C. Dubois, and M. Skorobogatiy, "Transmission measurements of hollow-core THz Bragg fibers," Journal of Optical Society of America, vol. 28, pp. 896-907, June, 2011.

58. M. Nagel, A. Marchewka, and H. Kurz, "Low-index discontinuity terahertz waveguides," Optic Express, vol. 14, pp. 9944-9954, July, 2006.

59. M. Uthman, B. M. A. Rahman, N. Kejalakshmy, A. Agrawal, K. T. V. Grattan, "Design and Characterization of Low-Loss Porous-Core Photonic Crystal Fiber," IEEE Photonic Journal, vol. 4, pp. 2315-2325, September, 2012.

60. S. Kaijage, ZhengbiaoOuyang, Xin Jin, "Porous-Core Photonic Crystal Fiber for Low Loss Terahertz Wave Guiding," IEEE Photonic Technology Letters, vol. 25, pp. 1454-1457, October, 2013.

61. A. Hassani, A. Dupuis, and M. Skorobogatiy, "Low loss porous terahertz fibers containing multiple sub wavelength holes," Appl. Phys. Vol. 92, pp. 071101, November, 2008.

62. S.-Y. Wang, "Microstructure optical fiber with improved transmission efficiency and durability," U.S. patent 6, pp.418, 258, July 9, 2002.

63. S. Atakaramians, S. AfsharVahid, B. M. Fischer, D. Abbott, and T. M.Monro, "Porous fibers: a novel approach to low loss THz waveguides, "Opt. Vol. 16, pp. 8845–8854, April 2008.

64. M. R. Hasan, M. A. Islam, and A. A. Rifat, "A single mode porous-core square lattice photonic crystal fiber for THz wave propagation," J. Eur.Opt. Soc. Rapid Publ. Vol. 12, no.15, pp.1–8, January 2016.

65. Raonaqul Islam, G. K. M. Hasanuzzaman, Md. Selim Habib, Sohel Rana, M. A. G. Khan, "Low-loss rotated porous core hexagonal single-mode fiber in THz regime," Elsevier Optical Fiber Technology, Vol. 24, pp. 38-43, August 2015.

66. Md.Saiful Islam, Sohel Rana, Mohammad Rakibul Islam, Mohammad Faisal, Hasan Rahman, Jakeya Sultana, "Porous core photonic crystal fiber for ultra-low material loss in THz regime,'' IET Communications, Vol.10, no.16, pp. 2179 – 2183, October 2016.

67. S. F. Kaijage, Z. Ouyang, X. Jim, "Porous-core photonic crystal fiber for low loss terahertz wave guiding," IEEE Photon. Technol. Lett., vol. 25, no. 15, pp. 1454–1457, Aug. 1, 2013.

68. M.A. Habib, M.S. Anower, M.R. Hasan, "Highly birefringent and low loss microstructure fiber for THz wave guidance", Opt. Communication, Vol. 423, pp.140–144, July 2018..

69. K. Nielsen, "Bendable, low-loss Topas fibers for the terahertz frequency range," Opt. Express, Vol. 17, no.10, pp. 8592–8601, August 2009.

70. H. Bao, "Fabrication and characterization of porous-core honeycomb band gap THz fibers," Opt. Express, Vol. 20, no.28, pp. 29507–29517, December 2012.

71. M.S. Islam, J. Sultana, J. Atai, D. Abbott, S. Rana, M.R. Islam, “Ultra low loss hybrid core porous fiber for broadband applications”, Appl. Opt. Vol. 56, pp. 1232–123, February 2017.
72. S. Rana, M.S. Islam, M. Faisal, K.C. Roy, R. Islam, S.F. Kaijage, “Single-mode porous fiber for low-loss polarization maintaining terahertz transmission”, Opt. Eng. Vol. 55, no. 7, pp. 076114, January 2016.
73. Roy, S., S. F. Kayser, and T. Azmaeen, "Design and optimization of a single mode octagonal photonic crystal fiber for high negative dispersion and high nonlinearity." In 2016 5th International Conference on Informatics, Electronics and Vision (ICIEV), pp. 614-619. IEEE, 2016.
74. Chowdhury, Sawrab, Shuvo Sen, Kawsar Ahmed, and Sayed Asaduzzaman, "Design of highly sensible porous shaped photonic crystal fiber with strong confinement field for optical sensing." Optic, Vol. 142,pp. 541-549, November 2017.
75. Md Sohidul Islam, K M Samaun Reza and Mohammad Rakibul Islam, “Topas based high Birefringent and low loss single mode hybrid porous core fiber for broadband application.” Indian Journal of Pure and Applied Physics Vol.56, pp.399-404, May 2018.
76. Hasanuzzaman, G. K. M., Sohel Rana, and Md Selim Habib, "A novel low loss, highly Birefringent photonic crystal fiber in THz regime." IEEE Photonics Technology Letters, Vol. 28, no. 8, pp. 899-902, October 2016.
77. Kawsar Ahmed, Sawrab Chowdhury, Bikash Kumar Paul, Md Shadidul Islam, Shuvo Sen, Md Ibadul Islam, and Sayed Asaduzzaman, "Ultrahigh birefringence, ultralow material loss porous core single-mode fiber for terahertz wave guidance." Applied optics, Vol. 56, no. 12, pp. 3477-3483, January 2017.
78. Md. Saiful Islam, Jakeya Sultana, Alex Dinovitser, Brian W-H. Ng, and Derek Abbott. "A novel Zeonex based oligoporous-core photonic crystal fiber for polarization preserving terahertz applications." Optics Communications, Vol. 413 pp. 242-248, January 2018.
79. Wu, Zhiqing, Zhaohua Shi, Handing Xia, Xiaoyan Zhou, Qinghua Deng, Jin Huang, Xiaodong Jiang, and Weidong Wu, "Design of highly birefringent and low-loss oligoporous-core THz photonic crystal fiber with single circular air-hole unit." IEEE

Photonics Journal, Vol. 8, no. 6, pp.1-11, February 2016.

80. Hasan, Md Rabiul, Md Shamim Anower, Md Ariful Islam, and S. M. A. Razzak. "Polarization-maintaining low-loss porous-core spiral photonic crystal fiber for terahertz wave guidance." Applied optics, Vol. 55, no. 15, pp.4145-4152, March 2016.

81. Luo, Jianfeng, Fengjun Tian, Hongkun Qu, Li Li, Jianzhong Zhang, Xinhua Yang, and Libo Yuan. "Design and numerical analysis of a THz square porous-core photonic crystal fiber for low flattened dispersion, ultrahigh birefringence." Applied optics, Vol. 56, no. 24, pp. 6993-7001,February 2018